

**DEVELOPMENT AND CHARACTERIZATION OF LIGHT
WEIGHT LAMINATED COMPOSITE UNDER IMPACT LOADING**

A Thesis
presented to
the Faculty of the Graduate School
University of Missouri-Columbia

In Partial Fulfillment
of the Requirements for the Degree
Master of Science

by
AJIT ABASO TAMBVEKAR

Dr. Sanjeev K. Khanna, Thesis Supervisor

DECEMBER 2013

The undersigned, appointed by the Dean of the Graduate School, have examined the dissertation entitled:

**DEVELOPMENT AND CHARACTERIZATION OF LIGHT
WEIGHT LAMINATED COMPOSITE UNDER IMPACT LOADING**

Presented by AJIT ABASO TAMBVEKAR

A candidate for the degree of Master of Science

And hereby certify that in their opinion it is worthy of acceptance.

Dr. Sanjeev K. Khanna

Dr. Robert Winholtz

Dr. Hani Salim

ACKNOWLEDGEMENTS

I would never have been able to finish my dissertation without the guidance of my committee members, help from friends, and support from my family and friends.

First and foremost, I would like to express my deepest gratitude to my advisor, Dr. Sanjeev K. Khanna, for his excellent guidance, caring, patience, providing me with an excellent atmosphere for doing research and also for patiently correcting my writing and financially supporting my research. Besides my advisor, my sincere thanks go to the rest of my thesis committee: Dr. Robert Winholtz and Dr. Hani Salim for permitting me to use their laboratories and also for their encouragements and insightful comments.

I would like to thank Hua Zhu, who as a good friend and as a lab-mate was always willing to help and give his best suggestions. It would have been a lonely lab without him.

I would also like to thank my parents and an elder brother. They were always supporting me and encouraging me with their best wishes.

Finally, I would like to thank my girlfriend, Manasi Kulkarni. She was always there cheering me up and stood by me through the good and bad times.

TABLE OF CONTENTS

| | |
|--|-----|
| ACKNOWLEDGEMENTS..... | ii |
| LIST OF ILLUSTRATIONS..... | vii |
| LIST OF TABLES..... | x |
| ABSTRACT..... | xi |
| 1 INTRODUCTION..... | 1 |
| 1.1 POLYURETHANE (PU)..... | 9 |
| 1.2 GRAPHENE (GR)..... | 11 |
| 1.3 GRAPHENE/POLYURETHANE COMPOSITE..... | 12 |
| 1.4 ALUMINUM ALLOYS | 14 |
| 1.4.1 Aluminum alloy 7075-T6..... | 15 |
| 1.4.2 Aluminum alloy 2024-T3..... | 16 |
| 1.4.3 Aluminum alloy 5052-H32 | 17 |
| 1.5 STEEL | 18 |
| 1.5.1 Main required properties for armor steels..... | 18 |
| 1.5.2 Typical properties of armor steels..... | 19 |
| 1.5.3 Martensitic steel | 20 |
| 1.5.4 Boron steel | 20 |

| | | |
|-------|---|----|
| 2 | EXPERIMENTAL METHOD | 22 |
| 2.1 | MATERIALS REQUIRED..... | 22 |
| 2.2 | FABRICATION PROCEDURE | 22 |
| 2.2.1 | Surface modification..... | 22 |
| 2.2.2 | Making mold for first layer..... | 25 |
| 2.2.3 | Making Composites of polyurethane and grapheme..... | 26 |
| 2.2.4 | Making mold for second layer | 28 |
| 3 | MECHANICAL TESTING..... | 30 |
| 3.1 | TENSILE TESTING..... | 30 |
| 3.1.1 | Introduction..... | 30 |
| 3.1.2 | Tensile Test Sample Preparation..... | 31 |
| 3.1.3 | Testing Procedure | 32 |
| 3.1.4 | Data analysis..... | 35 |
| 3.1.5 | Tensile Test Results | 38 |
| 3.2 | LAP SHEAR TESTING | 42 |
| 3.2.1 | Introduction..... | 42 |
| 3.2.2 | Specimen Preparation | 43 |

| | | |
|-------|---|----|
| 3.2.3 | Test Procedure | 44 |
| 3.2.4 | Lap Shear Test Results..... | 46 |
| 3.3 | THREE POINT BENDING TESTS | 49 |
| 3.3.1 | Introduction..... | 49 |
| 3.3.2 | Sample Preparation | 50 |
| 3.3.3 | Test apparatus and Procedure | 51 |
| 3.3.4 | Three Point Bend Test Results..... | 53 |
| 3.4 | FINITE ELEMENT MODEL OF THREE POINT BEND TEST | 53 |
| 3.4.1 | Introduction..... | 54 |
| 3.4.2 | Material Properties..... | 54 |
| 3.4.3 | Three Point Bend Test Modeling Approach | 60 |
| 3.4.4 | Three Point Bend Test Modeling Results | 63 |
| 3.5 | BALLISTIC TESTING | 67 |
| 3.5.1 | Introduction..... | 67 |
| 3.5.2 | Test configuration | 68 |
| 3.5.3 | Test Results..... | 68 |
| 4 | COLCLUSIONS AND FUTURE WORK..... | 71 |

5 REFERENCES..... 74

LIST OF ILLUSTRATIONS

| | |
|---|----|
| Figure 1.1 Laminated composite 1 (LC-1)..... | 7 |
| Figure 1.2 : Laminated composite 2 (LC-2). | 7 |
| Figure 1.3 : Laminated composite 3 (LC-3). | 8 |
| Figure 1.4 : Laminated composite 4 (LC-4). | 8 |
| Figure 1.5: General structure of a PU chain..... | 10 |
| Figure 1.6 : A view of a GR flat monolayer (Reproduced from [24]). | 11 |
| Figure 1.7 : GR building all graphitic forms: Wrapped to 0-D buckyballs, rolled to 1-D carbon-nanotubes, and stacked to 3-D graphite (Reproduced from [22]). | 12 |
| Figure 2.1 : Silaning steps..... | 24 |
| Figure 2.2: Mold preparation. | 25 |
| Figure 2.3 : Sonication apparatus..... | 26 |
| Figure 2.4 : Vacuum chamber for degasing..... | 27 |
| Figure 2.5 : Clamping the plates together..... | 28 |
| Figure 2.6 : 7 layered laminated composite..... | 29 |
| Figure 3.1: Tensile testing specimens of the martensitic steel and 0.5% PU/GR composite..... | 31 |

| | |
|--|----|
| Figure 3.2 : The martensitic steel sample loaded in a MTS load frame..... | 33 |
| Figure 3.3 : PU/GR tensile test specimen held in Instron load frame..... | 34 |
| Figure 3.4 : Engineering stress - strain curve for 0.5 % GR/PU composite..... | 38 |
| Figure 3.5 : Engineering stress - strain curve for the martensitic steel..... | 39 |
| Figure 3.6 : True stress-true plastic strain curve for 0.5% GR/PU composite..... | 41 |
| Figure 3.7 : True stress-true plastic strain curve for the martensitic steel..... | 41 |
| Figure 3.8 : Lap shear test specimen loaded in an Instron load frame..... | 45 |
| Figure 3.9 : Force vs. displacement graph for aluminum-PU/GR-aluminum samples..... | 46 |
| Figure 3.10 : Force vs. displacement graph for steel-PU/GR-aluminum samples..... | 47 |
| Figure 3.11 : Three point bend fixture..... | 50 |
| Figure 3.12 : Three point bend test set up on Instron testing machine..... | 52 |
| Figure 3.13 : Force vs. deflection of LC-1..... | 53 |
| Figure 3.14 : Engineering stress - strain curve for the boron steel..... | 56 |
| Figure 3.15 : Engineering stress - strain curve for Al 7075 T-6..... | 56 |
| Figure 3.16 : Engineering stress - strain curve for Al 2024 T-3..... | 57 |
| Figure 3.17 : Engineering stress - strain curve for Al 5052 H-32..... | 57 |
| Figure 3.18 : True stress-true plastic strain curve for the boron steel..... | 58 |

| | |
|---|----|
| Figure 3.19 : True stress-true plastic strain curve for Al 7075 T-6..... | 59 |
| Figure 3.20 : True stress-true plastic strain curve for Al 2024 T-3..... | 59 |
| Figure 3.21 : True stress-true plastic strain curve for Al 5052 H-32. | 60 |
| Figure 3.22 : ABAQUS model assembly..... | 61 |
| Figure 3.23 : Meshed ABAQUS model (zoomed for better view). | 63 |
| Figure 3.24 : Comparing the ABAQUS results with the experimental results for LC-1. | 65 |
| Figure 3.25 : Force vs. deflection plot obtained from ABAQUS FEM simulation. | 66 |
| Figure 3.26 : Picture showing entering projectile damage of strike face of LC-4. | 69 |
| Figure 3.27 : Picture showing projectile impact damage of rear face of LC-4. | 69 |
| Figure 3.28 : Picture showing entering projectile damage of strike face of LC-3. | 70 |
| Figure 3.29 : Picture showing projectile impact damage of rear face of LC-3. | 70 |

LIST OF TABLES

| | |
|--|----|
| Table 1.1 Mechanical properties of conventional armor steel (reproduced from steels for ballistic protection)..... | 19 |
| Table 3.1 : Ultimate tensile strength of the tested materials..... | 40 |
| Table 3.2: Shear area and lap shear strength of all the lap shear test specimens..... | 49 |
| Table 3.3 : Material properties used for ABAQUS modeling. | 55 |
| Table 3.4 : Bending stiffness of composite beams..... | 67 |

ABSTRACT

Today, armor protection is one of the most important elements of survivability. So developing materials which can withstand all futuristic threats, including those from terrorism has therefore become very critical. Polymer matrix composites (PMCs) are attractive materials in this regard because they are lighter, stronger, and stiffer than unreinforced polymers. Along with PMCs, steel and aluminum alloys are also used in light weight armor materials against projectile impact. The laminated composite materials in which different layers of different materials are bonded together are becoming a key material for future lightweight military, marine, and aerospace hardware as they incorporate high hardness and sufficiently high toughness simultaneously. In this study a layered composite panel of steel and aluminum layers has been bonded with graphene reinforced polyurethane.

Four types of laminated panels were fabricated with steel facing plate followed by a combination of various aluminum alloy layers. The average weight of a 7-layer laminated composite was 7 lb/ft² and that of 9-layer laminated composites was 10 lb/ft². Different tests, such as tensile test, lap shear strength test, and three-point bend test, have been conducted on the fabricated panels to determine their mechanical properties. The composite laminates' bending stiffness was modeled using ABAQUS finite element software and validated by experiments. The effect of a ballistic impact with armor piercing ammunition was also conducted to qualitatively measure their relative resistance to failure under ballistic loading.

1 INTRODUCTION

Today, armor protection is one of the most important elements of survivability. Casualties have become a cause for alarm and human life is taken as a very precious commodity. So developing the materials and modules which can withstand all futuristic threats, including those from terrorism has therefore become very critical. To protect the systems, new concepts in design and testing methods for optimizations of armor shall be developed. The total weight of the combat vehicle and the power-to-weight ratio has always been the constraint for the weight of the armor. The changing types of threats in recent years have led to a shift in focus on the need for protection against multi-spectral threats. Huge efforts are being put in all over the world to develop armor materials and systems providing greater ballistic protection with some increase in weight of the vehicle [1]. Today, no single material is able to effectively defeat a wide range of threats and hence, a wide variety of armors has to be developed [1]. Military vehicles are normally armored to withstand the impact of shrapnel, bullets, missiles, or shells, protecting the personnel inside from enemy fire. Some examples of such vehicles include tanks, aircraft, and ships. Civilian vehicles, which include cars used by reporters, officials and others in conflict zones or where violent crime is common and presidential limousines, may also be armored. Armored cars are also used by security firms to carry money or valuables to reduce the risk of highway robbery.

Armor may also be used in vehicles to protect from threats other than an intended attack. Some spacecraft are armed with specialized armor to protect them against impacts from micrometeoroids or fragments of space junk. The design and purpose of the vehicle depends on

the amount of armor plating carried, as the plating is often very heavy and excessive amounts of armor restrict mobility. In order to decrease this problem, some new materials (nanomaterials) and material compositions are being developed.

Composite materials have a wide range of engineering applications as they possess inherently superior mechanical properties, such as high strength-to-weight ratio and high stiffness, as aviation industry, civil, mechanical, defense, and other disciplines in which they are subjected to a wide spectrum of loading during in-service use. Today polymer matrix composites (PMCs) are one of the most attractive materials because they are lighter, stronger, and stiffer than unreinforced polymers or conventional metals, with the additional advantage that their properties and form can be tailored to meet the needs of a specific application [2]. High-performance nanoparticles such as carbon, silica, Kevlar, and graphene are of the highest interest for military and aerospace composite applications. PMCs have been widely used in military applications to resist foreign object impact loading. The property of PMC of retarding the projectile by absorbing its kinetic energy through different mechanisms such as deformation of the composite, delamination, and shear between layers makes them suitable to be incorporated in the materials resisting ballistic impacts [2]. The ballistic limit is certainly the most important factor for designing a suitable protective structure. Therefore, it is important to understand the behavior of composite structures under ballistic impact and the associated damage mechanisms in order to effectively utilize the composite as a protective structure.

Literature Review

The behavior of composite materials under impact loading has been studied to a large extent. However, the behavior of polyurethane/graphene nano-composites under ballistic impact is still not clearly understood.

Hazell et al. [3] have investigated the response of a bonded carbon—fiber-reinforced plastic composite panel to impact, penetration, and perforation by a high-velocity steel sphere. Zhu et al. [4] determined the ballistic limit and measured the terminal velocities of woven Kevlar/polyester laminates of varying thicknesses to quasi-static and dynamic penetration by cylindroconical projectiles. It was found that deliberately introduced delamination and changes in the volume fraction did not result in significant changes in the impact resistance. Cheng et al. [5] developed a model for high-velocity impact on thick composites for predicting the response of thick composite targets. The model was implemented into a hydrodynamic finite element code. It was reported that punching, fiber breakage, and delamination were the major energy-absorbing mechanisms of the penetration processes. Zhao et al. [6] investigated response of T300/epoxy composite laminates at different velocities of 10-300 m/s striking on 2.4 mm thick laminates having a stacking sequence of $[(45/-45)_4]$, $[(0/45/90/-45)_2]$ and 4.8 mm thick laminates having a stacking sequence as $[(0/45/90/-45)_4]$ and they measured three types of bullet striking velocities classified as less, equal, and larger than the ballistic limit velocity by a high speed gas gun. The whole penetration process was recorded by high-speed camera from the front side of targets, and then the fracture and the energy absorption of specimens were analyzed. The stress distribution was investigated through the reading of strain gages installed on specimens. Kumar et al. [7] investigated the ballistic response of thick Kevlar/epoxy laminated composite plates using numerical simulations. The ballistic impact caused by cylindrical projectiles at velocities between 100 and 1000 m/s was studied to find out the ballistic limit velocity, energy absorbed by the plate, and the contact duration. The effect of mass and diameter of the projectile on ballistic limit velocity was also studied. Ravid and Bodner [8] have developed a mathematical model for the penetration and perforation of visco-elastic metallic targets impacted with rigid projectiles using dynamic plasticity approach. They analyzed energy absorbed at different stages of penetration and perforation. They considered failure mechanisms like adiabatic shear failure, brittle shear

failure and tensile failure in their analysis. Tan and Khoo [9] studied ballistic properties of spectra shield laminates to by projectiles of flat-ended, hemispherical, ogival (CRH 2.5), and conical (300 half-angle) shapes. Spectra shield is a 0/90° flexible laminate of unidirectional Spectra-1000 fiber sandwiched between two thermoplastic films. The tests showed that the laminate is cut through a shearing action by flat-ended projectiles, whereas they are perforated by hemispherical projectiles by stretching the spectra filaments resulting in a rectangular hole in the laminates. On the other hand, obival and conical projectiles perforate the laminates with minimal delamination and tearing of the specimens. The area of the specimens affected by the projectiles appears to increase in size instead of becoming more localized at higher impact velocities.

Wang et al. [10] used nonlinear finite element software ANSYS/LS-DYNA to simulate the impact response of the sandwiched polyurethane composite steel tube as well as the traditional steel pipe. In the numerical simulation experiments, a sandwiched polyurethane tube and a steel tube with the same mass were respectively collided with rigid balls with the same velocity. It was concluded that the sandwiched polyurethane composite pipe are more crashworthy, have more deformation capacity, and have more collision energy absorption capacity than that of the traditional steel tube. In a study by Wentworth S.E. et al. [11] ballistic performance of series of polyurethane blocks has been synthesized and cast into 6'x6'x1/2' specimen for ballistic evaluation. The ballistic limit of the polyurethane cast sheet was carried out by 0.22 caliber projectiles with 0% obliquity. High speed photographs were taken for capturing the impact event. It was reported that the ballistic limit values of polyurethane are generally higher than that of polycarbonate and the response of polyurethane to ballistic impact is always ductile which is important because no dangerous secondary fragments are generated. It was concluded that polyurethane shows considerable potential for application in transparent armor systems. C. G. Fountzoulas et al. [12] studied the ballistic performance of laminates of polycarbonate (PC) and

polymethylmethacrylate (PMMA) with and without the presence of a polyurethane adhesive layer, using the nonlinear analysis software AUTODYN. 0.22-cal FSP projectiles were used at velocities of 173, 475, 846 and 1004 m/s. The simulation showed that the presence of the polyurethane adhesive layer provides an additional resistance to penetration, as witnessed by the experimentation.

Elastomeric polyurethane has always had the unique combination of high strength combined with very high strains at break (100s of percent). This basic property combination accounts for PUs enormous impact and abrasion resistance and energy absorbing capacity [13]. Elastomeric polyurethane is known to have good energy absorbing capacity. Therefore, it is a widely used material in ballistic applications [13].

Along with PMCs steel, aluminum alloys and ceramic materials are used as armor materials against bullets. At present, steel is the most common armor material and is extensively used for tanks and similar defense vehicles [14, 15]. A lot of work has been done to modify the performance of steel under ballistic impact.

Ubeyli et al. [16] studied the ballistic behavior of a laminated composite having an alumina front and dual phase steel backing layers by using 7.62 mm armor piercing (AP) projectiles under normal impact. The variables used were the martensite content of the backing layer and the areal density of the composite. Experimental results showed that utilization of a 6 mm thick alumina front layer, which was bonded to dual phase steel, enhanced the ballistic resistance of the dual phase steel remarkably. A study on the relationship between the material properties and the ballistic performance shows that increasing the hardness of the steel also increases the penetration resistance [15, 17]. Yilinaz et al. [14] experimentally investigated the performance of four types of boron alloyed armor steel plates with different types of heat treatments and eventually the

harnesses. All the plates were austenitized at 1000 °C for 45 minutes and quenched. The first plate was only treated for stress relief so that it reached the maximum hardness of HV 470. The remaining three were tempered at temperatures 540 °C, 600 °C and between 540 °C and 580 °C showing hardnesses of HV 443, HV 418, and HV 374 respectively. The ballistic perforation was carried out with the bullet having different velocities so that partial penetration to the complete penetration can be evaluated. The three plates with hardnesses HV 374, HV 418 and HV 443 were tested by the standard MIL-A-12 560. The results show that all the plates successfully passed the ballistic tests. After analyzing the perforation, it was reported that the opening whole size was increased as the hardness decreases.

High resistance of steels to ballistic impact depends on both a very high hardness and sufficiently high toughness and ductility for the armor not to get fractured by the impact and absorb maximum kinetic energy [18]. No material simultaneously possesses these properties. Hence the laminated composite materials in which different layers of different materials are bonded together is becoming the key development criteria for future lightweight military, marine, and aerospace hardware. Aluminum has excellent ballistic advantages due to its low density and high ductility, when utilized as primary armors on tactical trucks and combat vehicles [19].

To the author's knowledge, there is no literature available to investigate the high velocity ballistic response of a laminated composite having several layers of steel and aluminum and PU/graphene composite as an adhesive layer to bond the two metal plates together.

Project Objectives:

Thus, this study was conducted with four types of 12" x 12" laminated composites (LCs) as shown in Figures 1.1 to 1.4. A 2.4 mm layer of Polyurethane/graphene (PU/GR) composite has been used as an adhesive to bond two metal plates together. Figures 1.1 to 1.4 shows the

sequences in which the various metal plates are arranged in the four types of laminated composites. The martensitic steel and the boron steel, which forms first two layers, are to blunt the nose of the projectile which reduces the penetrating capacity of the projectile. The PU/GR composite layers help distributing the load over the larger plate area along with absorbing some part of energy by compression. The aluminum plates which form the back layers are to absorb the remaining energy of the projectile by ductile deformation.

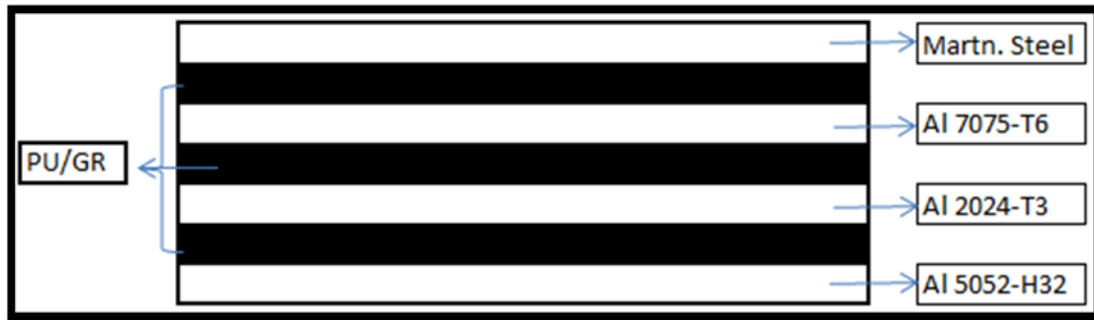


Figure 1.1 Laminated composite 1 (LC-1).

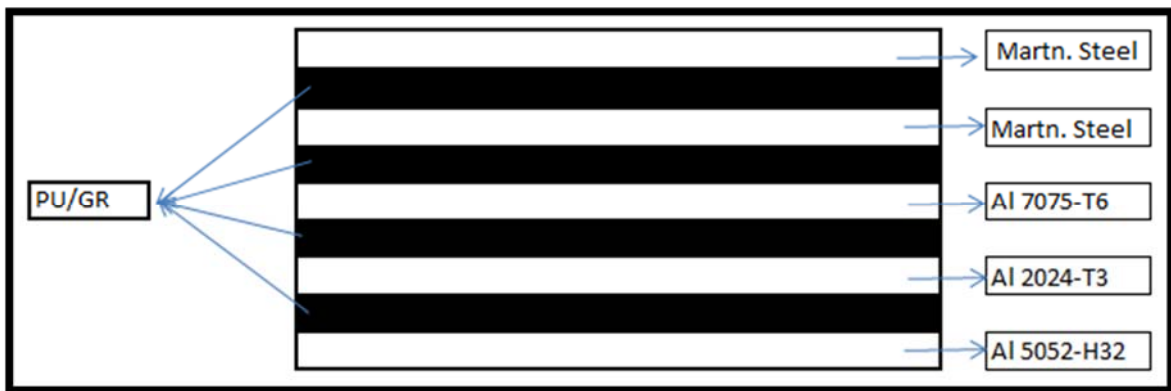


Figure 1.2 : Laminated composite 2 (LC-2).

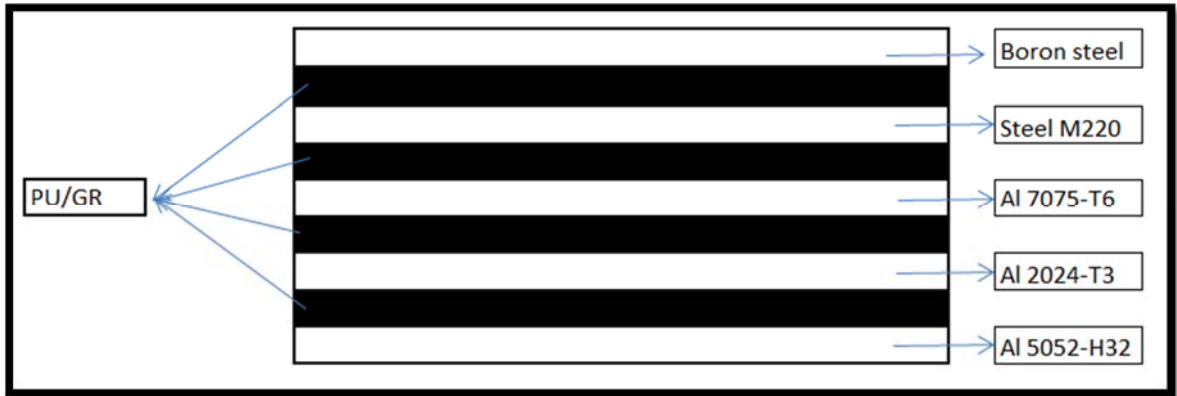


Figure 1.3 : Laminated composite 3 (LC-3).

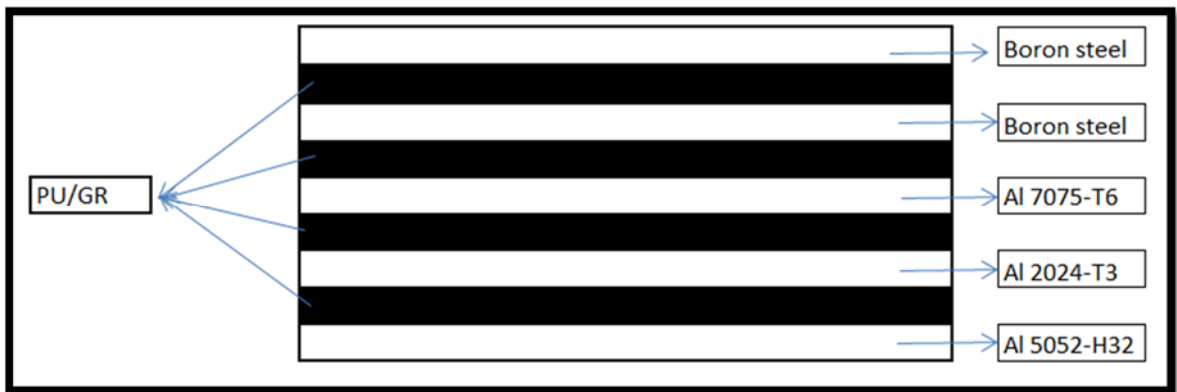


Figure 1.4 : Laminated composite 4 (LC-4).

The laminated composite LC-1 was tested under three point bending. Later, the three point bend test was modeled using the finite element program, ABAQUS, and bending behavior of all the four types of LCs were studied and compared to each other. A ballistic test was conducted on the laminated composites LC-4 and LC-3 per the ballistic testing standard BTS-005.

1.1 POLYURETHANE (PU)

PU has been known for nearly 60 years predominantly as elastomers and foamed materials. This study uses elastomeric PU consisting of chains of organic units joined by urethane links. As shown in Fig. 1.5, a PU chain consists of four basic components:

- 1) urethane groups,
- 2) di-isocyanate (NCO-R-NCO),
- 3) short-chain diols, the so-called chain extender (OHR'-OH) and
- 4) long chain diol (OH-----OH).

These components are divided into two separate phases: hard segment (HS) formed by the combination of diisocyanate and short-chain diols, and soft segment (SS) created by diisocyanate and long-chain diols. Conventionally, PU is named as segmented PU or copolymers. At room temperature, HS has high density and is rigid, while SS has very low density and is flexible. SS forms an elastomeric matrix responsible for elastic properties of PU, and HS acts as multifunctional tie points, functioning as both cross-links and reinforcing fillers. These physical cross-links recover the shape of SS continuous phase [20].

Unlike regular rigid plastics, PU is considered as one of the most versatile plastic materials with very high ductility and good stress-strain recovery [21]. When stretched or compressed beyond the elastic limit, PU shows resilience with no significant permanent deformation. On release of the applied strain PU tends to recover close to its original dimensions with little permanent set. Today, PU belong to the group of important materials applied in numerous fields of engineering

such as sandwiched composites, coatings, packing, cushioning, adhesives, and biomimetic materials.

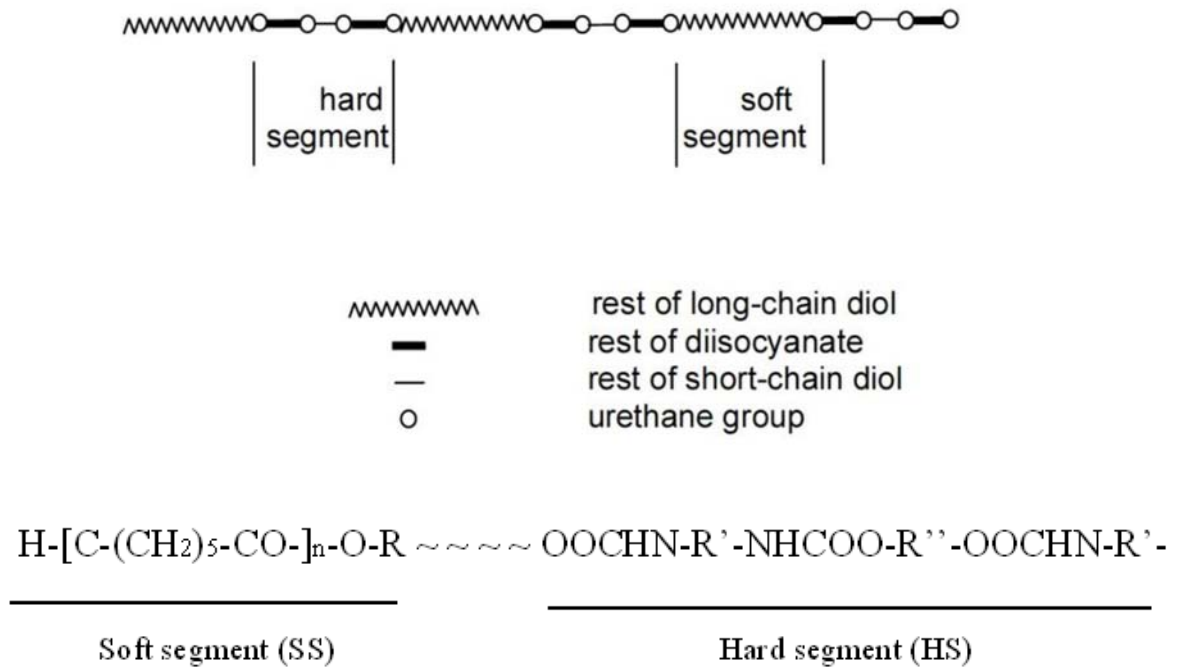


Figure 1.5: General structure of a PU chain.

The problem with PU is that it demonstrates low stiffness and low peak stress. Despite good deformability, these weak mechanical properties limit its uses in structural applications especially for PU with low HS content [22].

1.2 GRAPHENE (GR)

Graphene (GR), a new material introduced for the first time in 2004, is a flat monolayer of carbon atoms, tightly packed into a two dimensional honeycomb lattice as shown in Fig. 1.6. It is a basic structure unit, building 0D bucky balls, 1D carbon-nanotubes, and 3D graphite (Fig. 1.6) [23-25].

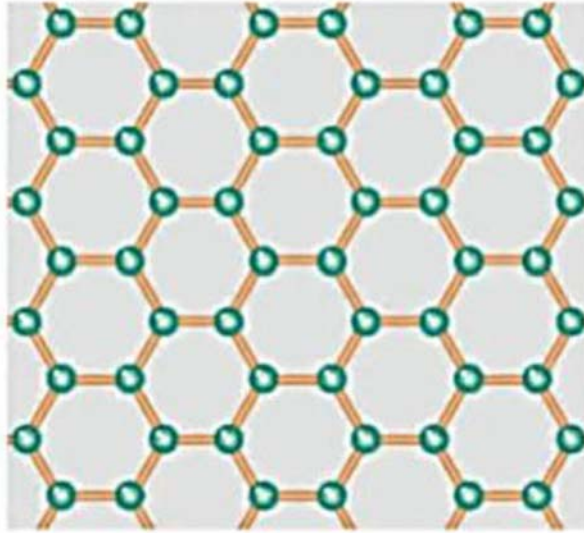


Figure 1.6 : A view of a GR flat monolayer (Reproduced from [24]).

GR appears to be an inexpensive material available in large quantities with a well-known potential effectiveness for improving mechanical, electrical, thermal and other properties [25]. For example, measurements have shown that GR has a breaking strength 200 times greater than steel, a bulk ultimate strength of 130 GPa, Young's modulus of 1,060 TPa, and a fracture strength of 125 GPa, making it one of the strongest materials ever tested. In electrical and thermal fields, GR has high electrical conductivity up to 6000 S/cm and thermal conductivity of 5000 W/m-K, which is ideal for use in atomically thin robust components for nanoelectronics [25]. These

properties make GR promising in many applications such as solar cells, hydrogen storage, sensors, batteries, super-capacitors and nanocomposites [26].

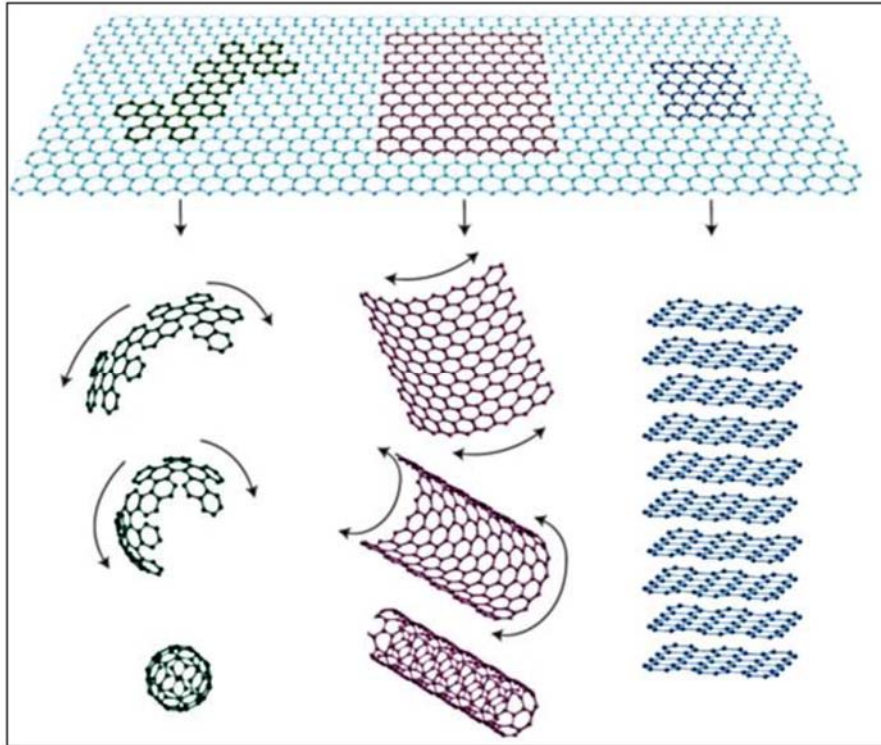


Figure 1.7 : GR building all graphitic forms: Wrapped to 0-D buckyballs, rolled to 1-D carbon-nanotubes, and stacked to 3-D graphite (Reproduced from [22]).

1.3 GRAPHENE/POLYURETHANE COMPOSITE

The discovery of nanoparticle-reinforced-polymer composite is one of the more important additions to the area of nanoscience in recent years because improvements can be obtained at very small filler loadings (up to 2%) in the polymer matrix, while traditional composite needs nearly 50%wt. of additional fillers [25]. Therefore, weak mechanical properties of PU can be improved by reinforcing with low volume fractions of rigid, impermeable nanofillers. For many

years, nanocomposites using carbon-nanotubes as reinforcing fillers have proven effective for improving mechanical properties of polymer matrix [21, 22, 27]. However, their difficulties are dispersion of carbon-nanotubes in polymer matrix and high costs. As mentioned, GR is relatively inexpensive, easily available, and well dispersed in polymer matrix by a solution mixing method, melt mixing, and in situ polymerization [26, 28, 29]. Besides, with the outstanding properties of GR and the ability to form chemical bonds by reaction between the diisocyanate groups of PU chains and hydroxyl groups on GR, it can be an effective nanofiller for PU matrix [25, 28]. Moreover, the major difference in properties of PU and GR is believed that the reinforcing effect will be significant.

A study [20] reports that the GR/PU composite is a strong strain-rate-dependent material, especially in the high strain rate regime of 3000 s^{-1} to 5000 s^{-1} . The dynamic mechanical properties of GR/PU composite in terms of plateau stress, peak stress, and peak load carrying capacity is better than that of pristine PU at most of applied strain rates. It is also stated that 0.5%wt GR is an ideal volume fraction added into PU matrix as 0.5%wt-GR specimen shows the maximum peak stress. At impact velocity of 25.664 m/s the maximum stress induced in 0.5%wt-GR specimen is found to be 268.6 MPa which is approximately 117% higher than pristine PU [20].

Along with being high energy absorbing material, PU happen to be a good adhesive to bond two metal plates together [30]. For this study, PU/graphene composites with 0.5%wt-GR is used as an adhesive to bond two metal plates together.

1.4 ALUMINUM ALLOYS

Aluminum is one of the most versatile existing metals as there exist a remarkable range of physical and mechanical properties that can be developed, from refined high-purity aluminum to the most complex alloys. More than three hundred alloy compositions are commonly recognized, and many additional variations have been developed internationally and in supplier/consumer relationships [31]. The properties of aluminum and its alloys that make it the most economical and attractive for a wide variety of applications are appearance, light weight, fabricability, physical properties, mechanical properties, and corrosion resistance. Aluminum has a density of only 2.7 g/cm³, approximately one-third as much as steel (7.83 g/cm³), copper (8.93 g/cm³), or brass (8.53 g/cm³). It can display excellent corrosion resistance in most environments, including atmosphere, water (including salt water), petrochemicals, and many chemical systems. There are two principal classifications of aluminum alloys, namely casting alloys and wrought alloys, both of which are further subdivided into the categories heat-treatable and non-heat-treatable. Cast aluminum alloys generally have lower tensile strengths than wrought alloys.

There has been a large increase in the demand for ballistic grade aluminum recently due to the excellent ballistic advantages of this low density metal when utilized as primary armors on tactical trucks and combat vehicles. These materials offer good tradeoffs against small arms and fragment protection, have relatively low cost per pound, have a large industrial base production capacity and have established fabrication, repair and maintenance facilities with trained personnel [19]. The ballistic advantages of aluminum over higher performance non-metallic systems are further illustrated when the armors are subjected to large blast and multiple, simultaneous fragment impacts from improvised explosive devices.

A number of commercial heat-treatable aluminum alloys have been used in military applications even though no ballistic specification exists. These include the 2024-T3 aluminum-copper alloys and the 7075-T6 aluminum-zinc alloys. The only high strength, wrought, 7000 series aluminum alloy with a military specification is the 7039 aluminum-zinc alloy, controlled by MIL-DTL-46063H(MR) [32]. The 7039 alloy was previously used on a number of US armored vehicles. The 7075 alloy is similar to 7039, but with higher strength[19]. As with 7039, the high strength 2024 and 7075 alloys have better ballistic protection against bullets than the 5083, 5059 and 6061 alloys, but suffer from large back plate spalling against large fragment impacts that causes unacceptable behind armor debris[19].

1.4.1 Aluminum alloy 7075-T6

Introduced by Alcoa in 1943, alloy 7075 has been the standard workhorse 7XXX series alloy within the aerospace industry ever since. It was the first successful Al-Zn-Mg-Cu high strength alloy using the beneficial effects of the alloying addition of chromium to develop good stress-corrosion cracking resistance in sheet products. Alloy 7075 sheet and plate products have application throughout aircraft and aerospace structures where a combination of high strength with moderate toughness and corrosion resistance are required. It is one of the commercially available heat-treatable aluminum alloys that have been used in military applications [19].

A study shows that 7075 alloys have provided ballistic protection against bullets than the 5083, 5059 and 6061 alloys and are comparable to 7039 aluminum-zinc alloy, which is 7000 series aluminum alloy with a military specification controlled by MIL-DTL-46063H(MR) [19]

The temper T6 designates that this alloy is solution heat treated and artificially aged. T-6 group encompasses products that are not cold worked after solution heat treatment and for which

mechanical properties or dimensional stability, or both, have been substantially improved by precipitation heat treatment [31].

For this study, 1/16" thick plates of 7075-T6, 2024-T3 and 5052-H32 were obtained from a supplier. The yield strength of 7075-T6 alloy is 516 MPa; ultimate tensile strength is 585 MPa and maximum elongation at break is 8%.

1.4.2 Aluminum alloy 2024-T3

Alloy 2024 was introduced by Alcoa in 1931 as an alclad sheet in the T3 temper. It was the first Al-Cu-Mg alloy to have a yield strength approaching 50,000-psi and generally replaced 2017-T4 (Duralumin) as the predominant 2XXX series aircraft alloy. With its relatively good fatigue resistance, especially in thick plate forms, alloy 2024 continues to be specified for many aerospace structural applications. It is one of the commercially available heat-treatable aluminum alloys that have been used in military applications [19].

A study shows that 2024 alloys have better ballistic protection against bullets than the 5083, 5059 and 6061 alloys and are comparable to 7039 aluminum-zinc alloy, which is 7000 series aluminum alloy with a military specification controlled by MIL-DTL-46063H(MR) [19]

The temper T3 designates that this alloy is solution heat treated, cold worked, and naturally aged to a substantially stable condition. This temper applies to alloys that are cold worked to improve strength after solution heat treatment and for which mechanical properties have been stabilized by room-temperature aging [31].

For this study, 1/16" thick plates of 2024-T3 were obtained from a supplier. The yield strength of this alloy is 337 MPa; ultimate tensile strength is 462 MPa and maximum elongation at break is 10%.

1.4.3 Aluminum alloy 5052-H32

Aluminum 5052 is an aluminum magnesium alloy which can be hardened by cold work. It is not heat treatable to higher strength. It is about mid-way through the series of aluminum magnesium alloys for alloying content and strength. It has excellent fatigue properties, with an endurance limit of 115 MPa in the H32 temper. Aluminum alloy 5052 contains nominally 2.5% magnesium & 0.25% chromium. It has good workability, medium static strength, high fatigue strength, good weldability, and very good corrosion resistance.

The temper H32 designates that this alloy is strain-hardened and stabilized. This temper applies to products that are strain-hardened and whose mechanical properties are stabilized by a low-temperature thermal treatment or as a result of heat introduced during fabrication. Stabilization usually improves ductility. This designation applies only to those alloys that, unless stabilized, gradually age soften at room temperature. The digit following the H3 indicates the degree of strain hardening remaining after stabilization [31].

For this study, 1/16" thick plates of 5052-H32 are obtained from a supplier. The yield strength of this alloy is 160 MPa; ultimate tensile strength is 228 MPa and maximum elongation at brake is 11%.

1.5 STEEL

To provide protection against increasingly efficient battle field weapons, attempts are being made to enhance ballistic protection by using more and more efficient materials. Among such materials, the steel, which is the oldest of armor materials, has developed quite significantly so that it is still now the most extensively used material for ballistic protection problems [18]. Better knowledge of metallurgical parameters affecting the ballistic behavior of armor steels and substantial improvements in the manufacturing techniques of such steels have resulted in the production of new types of armor steels [18]

1.5.1 Main required properties for armor steels

A study [18] on armor steels and their properties shows that, a steel should have the following properties when it is used for the fabrication of armor vehicles.

a) high resistance to perforation and ballistic impacts

A study by Manganello and Abbott [33] investigated the effect of steel properties on the low velocity impact behavior of steel armors. They found that the hardness was the most critical parameter affecting the ballistic performance of the steels [33].

As a very general rule, to resist to projectile perforation, armor steel should have a high hardness. But there is no simple correlation between hardness and resistance to perforation. The steel's chemical composition and heat treatment (quench and temper) are varied to obtain the required hardness level.

b) High resistance to ballistic impacts

It is generally considered that armor steels should have a high toughness to resist ballistic impacts without being cracked or fractured.

1.5.2 Typical properties of armor steels

At present US military standard MIL-A-12560 specifies armor steel widely used at many applications. The steels according to us military standard MIL-A-46100 have a high hardness and their ballistic protection against of 12.5 mm armor prancing (AP) is by 20 % more efficient than those according to the standard MIL-A-12560[14]. These kind of steels have alloying elements such as manganese, sulphur, nickel, phosphorus, silicon, chromium, molybdenum and micro-alloying elements such as boron, aluminum, titanium, vanadium etc. The mechanical properties of several traditional armor steels are given in Table 1.1.

Table 1.1 Mechanical properties of conventional armor steel (reproduced from steels for ballistic protection).

| Armor Steel | Hardness Range (Brinell) | Mechanical Properties | | |
|-------------|-----------------------------|-----------------------|--------------|--------------------|
| | | Tensile properties | | |
| | | YS (MPa) | UTS (MPa) | elongation in % |
| MARS 190 | 375 | 1150 | 1250 | 14 |
| MARS 240 | 500 | 1350 | 1750 | 13 |
| MARS 270 | 550 | 1500 | 1900 | 10.5 |
| MARS 300 | 600 | 1600 | 2200 | 7 |

1.5.3 Martensitic steel

Martensitic stainless steels are low carbon steels with composition of iron, 12% chromium, and 0.12% carbon. They are usually tempered and hardened. Tempered martensite gives steel good hardness and high toughness. Untempered martensite is low in toughness and therefore brittle[34]. These steels offer much higher strength-to-weight ratios than conventional cold rolled steels and are more cost effective than other metals or plastics.

For this study, 2 mm thick plates of a tempered martensitic steel are used. The yield strength of this alloy is around 1400 MPa, ultimate tensile strength is around 1600 MPa and maximum elongation at break is around 6%.

The martensitic stainless steel used for this research is produced using low-carbon compositions strengthened with manganese (Mn), silicon (Si). It is considered to be one of the hardest categories of steels.

1.5.4 Boron steel

The boron steel used in this research is a hardenable boron alloyed steel coated with Al-Si coating. Aluminum-silicon coating protects steel from oxidation during heating and provides corrosion protection for the component. Boron as an alloying element significantly enhances the hardenability of the steel.

These steels are designed to be heat treated and then quenched during the hot stamping process. The mechanical properties of the final part make significant weight savings possible (up to 50% compared to standard high yield strength steel). One of the main advantages of the boron steel is

that it has exceptional fatigue and impact strength allowing substantial thickness and hence weight reduction.

For this study, 2 mm thick plates of the boron steel are used. The yield strength of this alloy is around 1100 MPa; ultimate tensile strength is around 1400 MPa and maximum elongation at break is around 8%.

2 EXPERIMENTAL METHOD

This chapter describes the process followed for fabrication of the laminated composites.

2.1 MATERIALS REQUIRED

Below is the list of required materials for carrying out the fabrication of laminated composite.

1. 12" x 12" x 0.0781" martensitic steel plate.
2. 12" x 12" x 0.0781" boron steel plate.
3. 12" x 12" x 0.0625" plates of aluminum 7075 T-6, aluminum 2024 T-3, aluminum 5052 H-32.
4. Polyurethane part A (ultralane 720 LV-A), polyurethane part B (ultralane 720 LV-B) and 25 nm sized graphene nanoparticles
5. Silane B2408 (Bis(2-hydroxyethyl)-3-aminopropyltriethoxysilane)

2.2 FABRICATION PROCEDURE

2.2.1 *Surface modification*

The PU/GR composite are used as an adhesive layer between two metal plates in the laminated composite. In this step the surface of the plates is modified for the better adhesion between metal plates and PU/GR composite. The procedure is as follows.

1. The first step in surface modification is to sand the bonding surfaces of metal plates with 100 grit aluminum oxide sand paper since roughening the surface increases the surface area and eventually the bond strength.
2. The second step is to treat the surface of all the plates with silane. This procedure is known as silaning.

The general formula of an organosilane ($R_nSiX(4-n)$) shows two classes of functionality. The X functional group is involved in the reaction with the inorganic substrate. The bond between X and the silicon atom in coupling agents is replaced by a bond between the inorganic substrate and the silicon atom. X is a hydrolyzable group, typically, alkoxy, acyloxy, amine, or chlorine. In this case Bis(2-hydroxyethyl)-3-aminopropyltriethoxysilane is used as a coupling agent and it has amine as the hydroxylable group. So in the present case, silane reacts with the metal oxide on the surface of metal plate and the bond between Si and hydroxylable group is replaced by Si-O bond. R is a nonhydrolyzable organic radical that possesses a functionality which enables the coupling agent to bond with organic resins and polymers. In the present case, R forms chemical bond with the polyurethane creating a strong adhesion between metal plate and polyurethane composite.

The procedure of silaning is as follows.

- a) Silane is added to a 95% ethanol – 5% water solution with stirring to yield a 2% final concentration.
- b) Five minutes should be allowed for hydrolysis and silanol formation.
- c) The plates are dipped into the solution, agitated gently, and removed after 1 – 2 minutes.



Figure 2.1 : Silaning steps.

- d) They are rinsed free of excess materials by dipping briefly in ethanol.
- e) The silane layer is cured for 5 – 10 minutes at 110°C or for 24 hours at room temperature.

2.2.2 Making mold for first layer

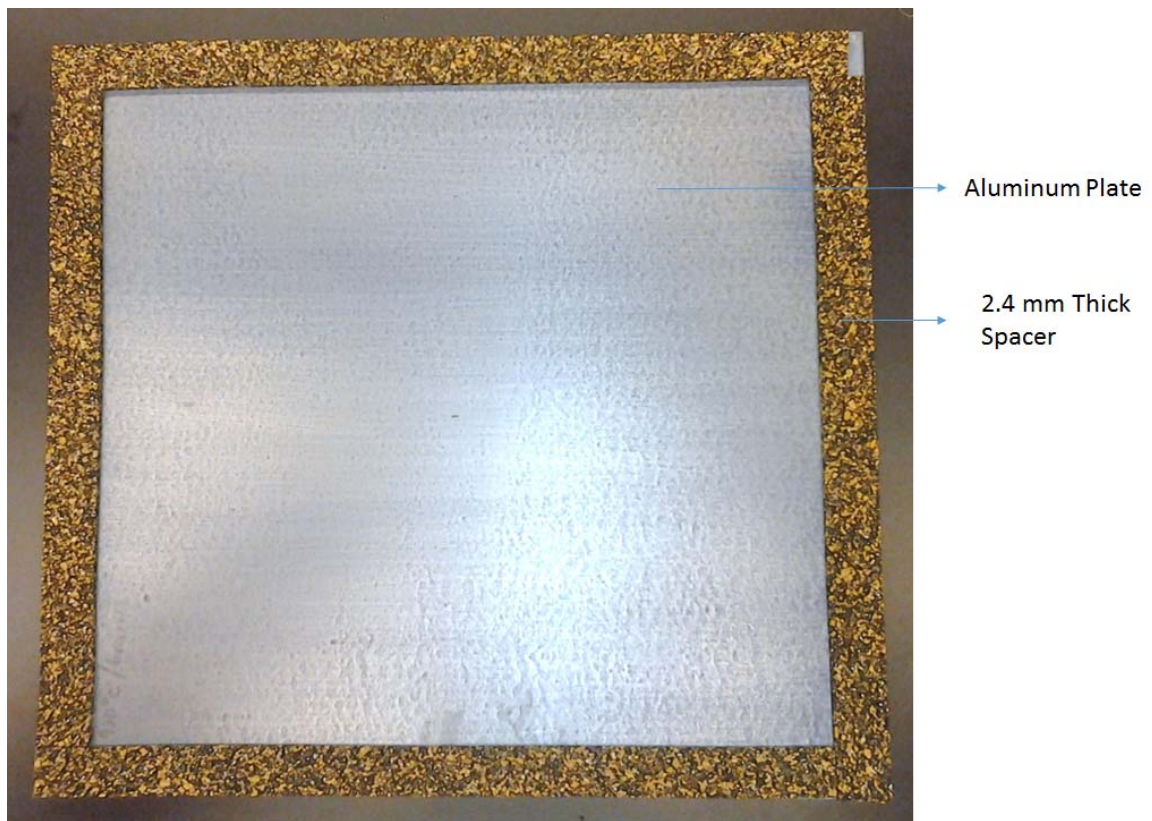


Figure 2.2: Mold preparation.

The PU/GR composite is itself acting as an adhesive between the two metal plates. The PU/GR composite is in liquid form when prepared and takes 36 hours for solidifying, curing and hardening. Mold on the metal plate face is required to hold the liquid in its position without leaking out. The rectangular cross sectioned 2.4 mm rubber strips are used to make the mold. Figure 2.2 shows the mold on aluminum plate.

2.2.3 Making Composites of polyurethane and graphene

As mentioned earlier, PU/GR composite is an adhesive as well as an energy absorbing layer in the laminated structure. Below is the procedure followed for making PU/GR composite in the laboratory. 0.5% graphene by weight was added to the PU matrix. Only 0.5% graphene was used based on the investigation by Phan [20] which reported that 0.5% GR/PU composites have the highest strength under high strain rates for graphene reinforced in the range of 0% to 1%.

1. Add required amount of graphene and acetone into a medium-sized beaker, stir the mixture for 2 minutes, put the medium-sized beaker into a bigger beaker, pour some ice water into the big beaker through the gap between two beakers, and then sonicate the mixture as shown in Figure 2.3.

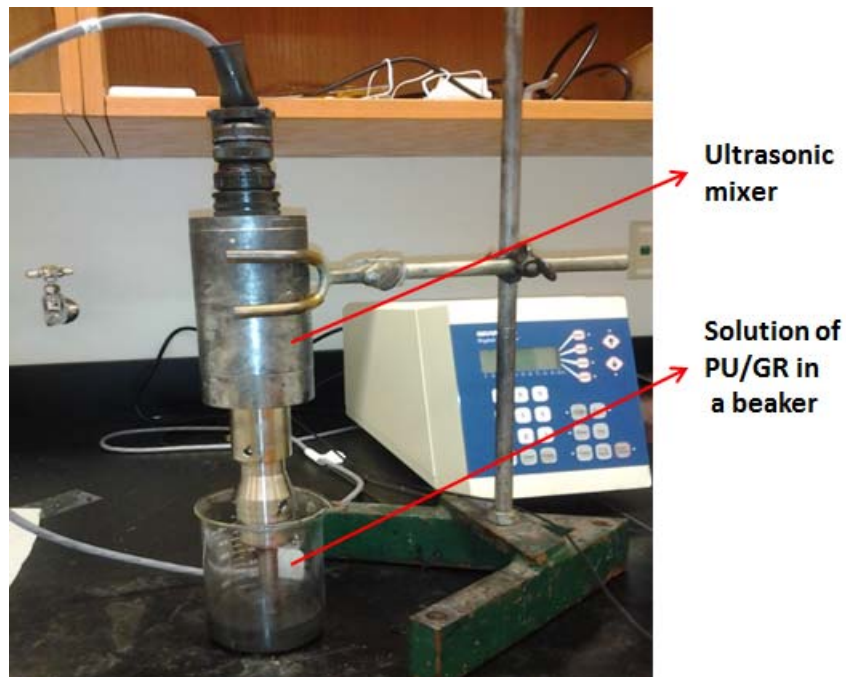


Figure 2.3 : Sonication apparatus.

2. After the sonication, get the medium-sized beaker out from the big beaker, pour polyurethane part A into the mixture, change the ice water in the big beaker, put the medium-sized beaker back into the big beaker, then sonify the mixture by using ultrasonic mixer. After sonification, get beaker A (medium-sized beaker contains polyurethane part A) out from the big beaker.
3. Repeat above procedures, for polyurethane part B.
4. Vacuum beaker A and beaker B at -29.0 bar for 15 to 20 min.
5. Pour beaker B into beaker A, change the ice water in the big beaker, put beaker A back into the big beaker, then sonify the solution by using ultrasonic mixer.
6. After sonication, get beaker A out from the big beaker, change the ice water in the big beaker, put beaker A back into the big beaker, put the big beaker into the vacuum chamber, vacuum the solution at 29.0 mmHg for 15 min.

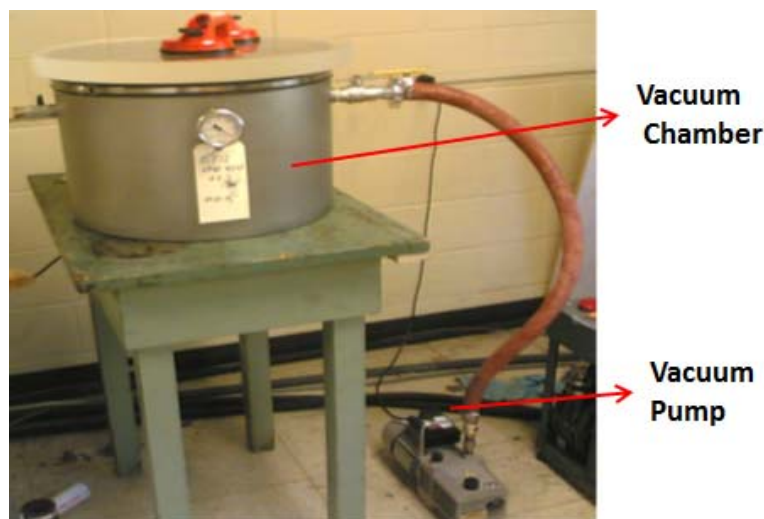


Figure 2.4 : Vacuum chamber for degasing.

After the PU/GR composite is made, it is poured into the mold. Care should be taken that the liquid is spread evenly and it is overflowed a little. It is recommended to wait for five minutes after the composite is poured into the mold to place the other plate on the top. This will help to get rid of acetone on the surface of the poured layer.

The next step is to put another plates on this plate. This should be done slowly starting from at an angle which will make the way for the air to go out and reduces the risk of air bubble getting trapped into the PU/GR composite. Both the plates with PU/GR composite layer in the middle are clamped to each other using C clamps, as shown in the figure 2.5.

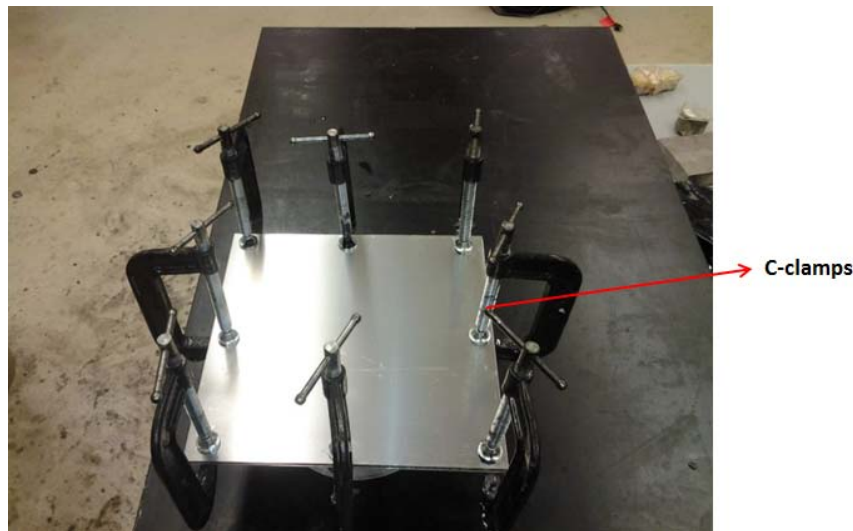


Figure 2.5 : Clamping the plates together.

2.2.4 Making mold for second layer

The PU/GR composite takes 36 hours for curing. The minimum wait time for building another layer is 12 hours. After 12 hours, a mold is made on the surface of the three layered laminated composite and then the same procedure is followed to make 7 layered and then 9

layered composite plates. Figure 2.6 shows the 7 layered laminated composite fabricated using this procedure.

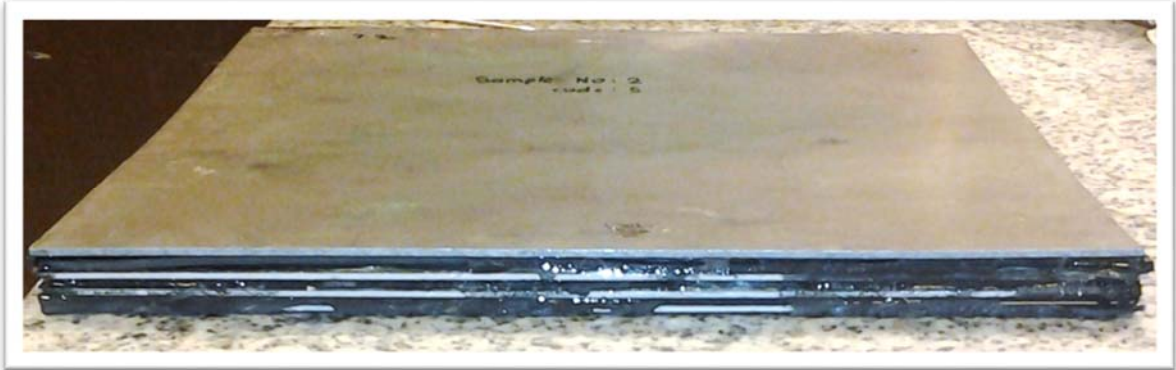


Figure 2.6 : 7 layered laminated composite.

3 MECHANICAL TESTING

3.1 TENSILE TESTING

3.1.1 Introduction

Tensile testing is one of the most fundamental tests for engineering materials, and provides valuable information about a material and its associated properties. These properties can be used for design and analysis of engineering structures, and for developing new materials that better suit a specified use. A laminated composite contains several layers of metal plates and PU/GR composite. Mechanical properties of all the materials in the laminated composites were required for the ABAQUS simulation of three point bending test of the laminated composite. All the metal plates have been obtained from suppliers. The mechanical properties of all metal plates except the martensitic steel have been provided by the supplier of the plates. So knowing the mechanical properties of the martensitic steel and PU/GR composite were essential.

3.1.2 Tensile Test Sample Preparation



Figure 3.1: Tensile testing specimens of the martensitic steel and 0.5% PU/GR composite.

Two different tensile testing machines were used for conducting tension tests. An Instron load frame and Instron 8800 data acquisition system were used for 0.5% GR/PU composite and an MTS load frame and data acquisition system were used for the martensitic steel. The samples were rectangular in cross section, with a reduced gage section. The reduced gage section ensured that the highest stresses occurred within the gage, and not near the grips of the load frame, preventing strain and fracture of the specimen near or in the grips.

Tensile testing of the martensitic steel was carried out per standard ASTM E8 [35]. Two dog bone shaped tensile test specimens were cut out of 12" x 12" plate of the martensitic steel by the water jet cutting. Tensile test of PU/GR composite was carried out per standard ASTM D638[36]. Three dog bone shaped tensile test specimens were fabricated using the standard mold of dog

bone samples which conforms to all the sample requirement of ASTM D638. Even a small crack in the gage length can cause stress concentration at that region and sample may break abruptly. To avoid this before testing, all the PU samples were sanded by using fine grit sand papers to remove burr and cracks, if any, on the cross-section of the specimens.

Three samples of PU and two samples of the martensitic steel were tested in the Instron load frame and MTS load frame respectively. After the tests, the data gathered into an Excel spreadsheet was used to calculate various properties of each material, including the elastic modulus, yield strength, ultimate tensile strength, true stress and true strain.

3.1.3 Testing Procedure

Each specimen was measured with calipers to determine the width and thickness. A gage length was determined (typically 50.00 mm) and marked into the specimen so that the distance between the two marks could be measured after the tensile test was completed. The data acquisition software was started, and the load cell was zeroed to ensure that the software only measured the tensile load applied to the specimen. The specimen was loaded into the jaws of the respective load frame so that it was equally spaced between the two clamps. The axial and transverse strain gages, along with axial extensometer were used to measure the strains in steel samples. Axial extensometers were used for measuring strain in PU samples.



Figure 3.2 : The martensitic steel sample loaded in a MTS load frame.



Figure 3.3 : PU/GR tensile test specimen held in Instron load frame.

The specimen was properly loaded in the frame and ensured that it wasn't slipping in the jaws. The load was released, and the extensometers were zeroed using the software. The test was started, and the specimen was loaded, resulting in a measureable strain. For all the samples, the crosshead was set to move downwards at 0.25 mm/min. The data was gathered using the software, and transferred into a spreadsheet. The test continued until fracture, where the software stopped the moving crosshead and finished gathering data. The specimen was removed and the crosshead was reset to the initial position to start another tensile test. The testing procedure was repeated for the rest of the specimens. Figures 3.2 and 3.3 shows the martensitic steel specimen loaded on MTS load frame and PU/GR specimen loaded on Instron load frame respectively.

3.1.4 Data analysis

3.1.4.1 Engineering Stress and Engineering Strain

Each material was tested and the Engineering stress-strain curves were plotted. To calculate the engineering strain on the Instron machine, we used extensometers and on the MTS machine, we used both axial extensometer and axial and lateral strain gauges, which measured the strain induced in the sample. The load cell on the moving crosshead measured the vertical load applied to the sample.

The cross section of the gage length on the sample was measured using calipers, and from there the area was calculated using Equation (3.1), where w denotes the width and b denotes the breadth of specimen. The engineering stress is a function of the force applied and the original cross-sectional area of the gage length of the sample. Using Equation (3.2), the engineering stress was calculated. P denotes the tensile force applied to the specimen.

$$A_o = w \times b \quad 3.1$$

$$\sigma = \frac{p}{A_o} \quad 3.2$$

3.1.4.2 Determining the Modulus of Elasticity and the Yield Stress

The modulus of elasticity and the yield strength was calculated for the martensitic steel and PU/GR composite. To find the modulus of elasticity, a small portion of the stress-strain curve was plotted to only include the linear region around zero strain. The slope of the graph at this point is the modulus of elasticity for that material. Excel was used to plot this portion of the stress-strain curve, and a trend line was added to best fit the data. Using the modulus of elasticity, the yield stress was also found. A straight line was plotted with the modulus of elasticity as the slope, but it was offset 0.002 mm/mm of strain in case of the martensitic steel and 0.02 mm/mm of strain in case of PU/GR sample. The value of the stress where the two lines cross is the corresponding yield stress. This method is the standard offset method used to find the yield stress.

The ultimate tensile strength was found by determining the maximum load, and using Equation 3.2 to solve for the maximum engineering stress encountered.

3.1.4.3 Determining the True Stress and the True Strain

The true stress and true strain was calculated for the martensitic steel and PU/GR composite samples. The engineering stress and strain does not account for the reduction in area as the sample is loaded, nor does it account for strains besides the axial direction. The true stress and true strain show the actual stress and strain encountered during the tensile test.

The true stress can be calculated at any point using Equation (3.3), but since the instantaneous area $A_{instant}$ was not known for this test, other methods had to be incorporated.

$$\sigma_{true} = P/A_{instant} \quad 3.3$$

For strains below two times the yield strain, the true stress is well approximated by the engineering stress σ . Between two times the yield strain and necking (the strain at the ultimate tensile stress), the true stress is approximated by Equation (3.4). σ is the engineering stress, and ϵ is the engineering strain.

$$\sigma_{true} = \sigma (1 + \epsilon) \quad 3.4$$

The true strain and true plastic strain were calculated using Equation (3.5) and (3.6) respectively. ϵ_{pl} denotes true plastic strain and E denotes the elastic modulus of the material. The first nonzero true stress is divided by the first nonzero true strain to calculate the elastic modulus of the material.

$$\epsilon_{true} = \ln(1 + \epsilon) \quad 3.5$$

$$\epsilon_{pl} = \epsilon_{true} - \frac{\sigma_{true}}{E} \quad 3.6$$

3.1.5 Tensile Test Results

3.1.5.1 Engineering Stress and Engineering Strain

The data from the tensile tests was plotted on separate graphs according to material. Each graph shows the engineering stress versus the engineering strain. Figure 3.4 shows the stress-strain curve for the 0.5 % GR/PU composite specimens, and figure 3.5 shows the stress-strain curve for the martensitic steel specimens.

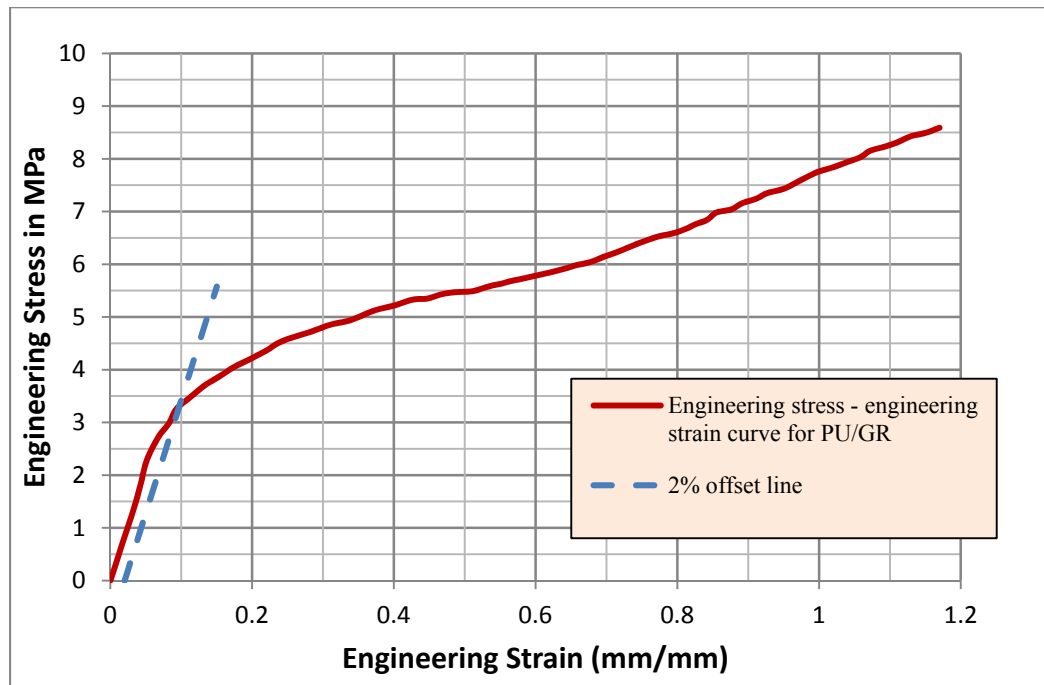


Figure 3.4 : Engineering stress - strain curve for 0.5 % GR/PU composite.

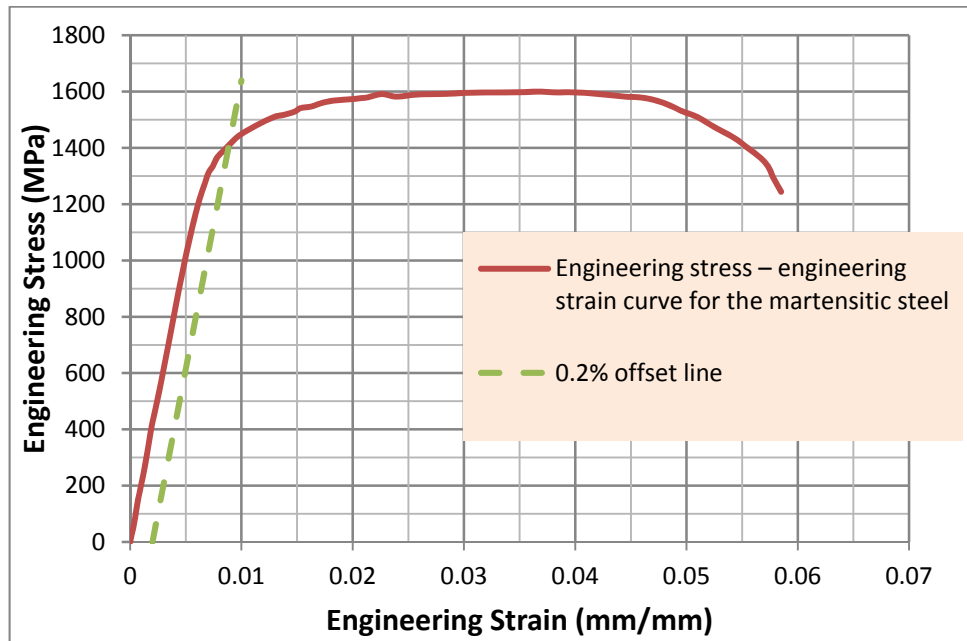


Figure 3.5 : Engineering stress - strain curve for the martensitic steel.

3.1.5.2 Material Properties

The ultimate tensile strength for each material is listed in Table 3.1. The value of the ultimate tensile strength was found using the procedure outlined in 1.1.4.2 section. The strain corresponding to the ultimate tensile strength is where necking begins to occur. The modulus of elasticity and the yield strengths were calculated for both the samples. Table 3.1 shows these values for both the materials.

Table 3.1 : Ultimate tensile strength of the tested materials

| Sample Material | Ultimate Tensile Strength (MPa) | Modulus of Elasticity (MPa) | Yield Strength (MPa) |
|------------------------|--|------------------------------------|-----------------------------|
| Martensitic steel | 1600 | 204968 | 1400 |
| 0.5% GR/PU | 8.59 | 42.905 | 3.2 |

3.1.5.3 True Stress and True Strain

The engineering stress and strain does not account for the change in cross sectional area, and only accounts for the axial strain in the sample. The true stress and strain account for the change in cross sectional area, and therefore the true stress is higher than the engineering stress. The true strain is also greater than the engineering strain due to strains in the transverse direction along the gage of the sample. Figure 3.6 shows true stress versus true plastic strain curve for 0.5% GR/PU sample and Figure 3.7 shows the true stress versus the true plastic strain curve for the martensitic steel.

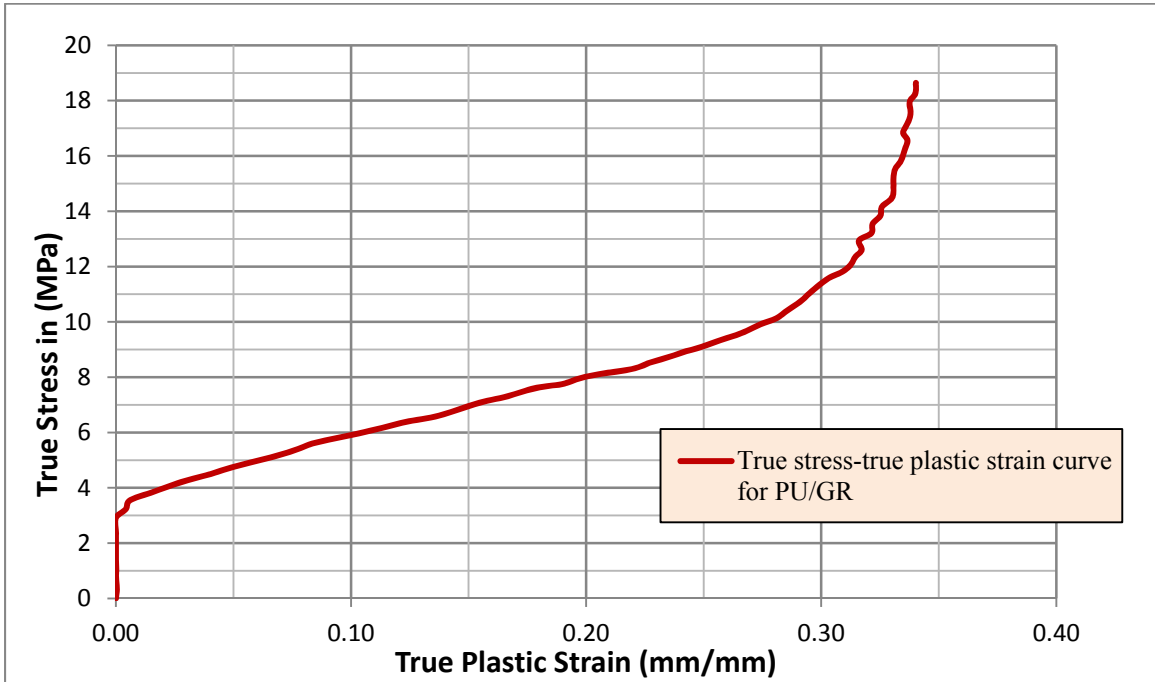


Figure 3.6 : True stress-true plastic strain curve for 0.5% GR/PU composite.

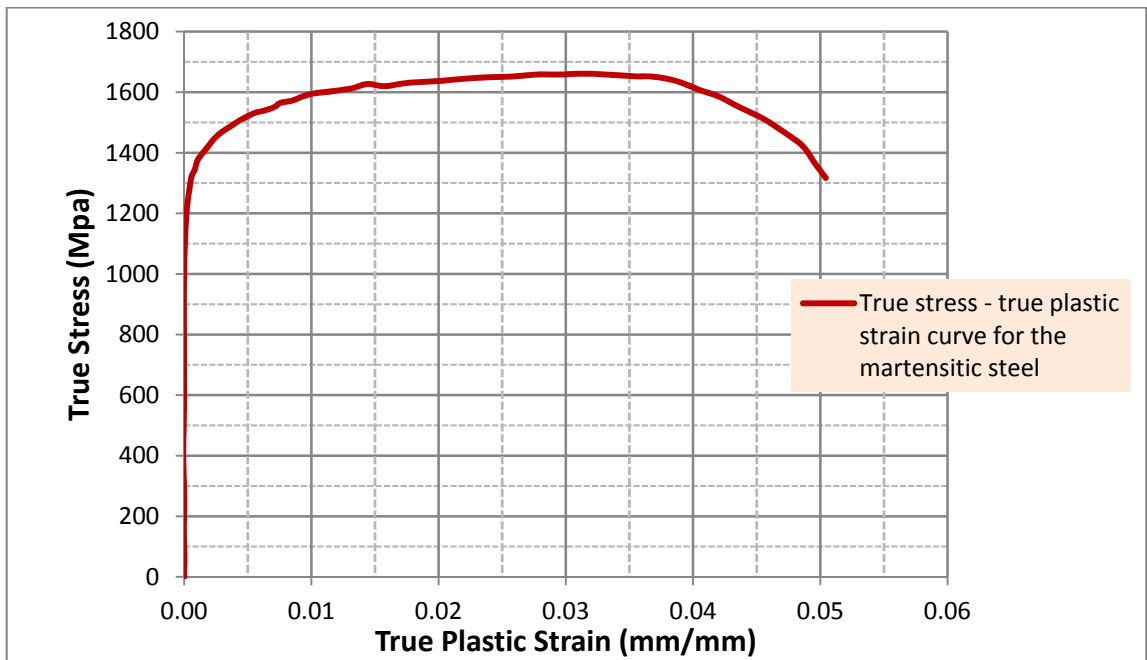


Figure 3.7 : True stress-true plastic strain curve for the martensitic steel.

3.2 LAP SHEAR TESTING

3.2.1 Introduction

Lap Shear tests are a common way to determine the shear strength of adhesives used for bonding materials such as plastics and metals. The test method is primarily used for qualitative comparisons. The test is applicable for determining adhesive strength and adhesive environmental durability. Lap shear strength is used to determine the maximum shear force required to fracture a sample. This process is similar to conventional tensile test. Mating lap shear panels are coated and adhesively bonded to each other. A tensile testing machine is used to apply the required load.

An adhesive bonded structure generally consists of three components of different mechanical properties namely the two adherents and the adhesive layer. The strength of an adhesive joint is not a property of the adhesive alone but depends on many factors like the adherents, the adhesive, the joint geometry, preparation of specimens and service conditions. The geometrical parameters that influence the strength of an adhesive are the length of the specimen, the length of the bonded portion of the overlap, crack length and the thickness of the adherends. The single lap joint is quite sensitive to changes in geometrical parameters. Metal-Metal bond Lap shear tests are generally carried out in accordance with ASTM D 1002-10 [37].

Laminated composite materials are made up of several layers of different materials. Testing the bond strength between two layers in the laminated composite is essential for knowing the tangential behavior of them under quasi-static or impact loading. The shear strength thus obtained from the test will be used for defining the interaction properties between the two mating surfaces in FEM simulation of the three point bending using ABAQUS. In this research 0.5% GR/PU resin was used as adhesives in making the lap joint. The major failure mode of the joints using these

resins is adhesive failure. Adhesive failure can be reduced by surface preparation of adherends while the cohesive failure depends on the strength of the resins.

3.2.2 Specimen Preparation

The test specimens were prepared by taking steel and aluminum plates of size 4" x 1", having a thickness of 1/8" and bonded together with PU/GR composite. The bond length, width and thickness are 0.5", 1" and 3/32" respectively. The following two types of test specimens were fabricated.

- 1) Steel bonded to aluminum with 0.5% GR/PU composite
- 2) Aluminum bonded to aluminum with 0.5% GR/PU composite

The procedure followed for sample preparation is as follows

1. Cut 4" x 1" strips from steel and aluminum plates
2. Sand the bonding surface of the plate using 100 grit aluminum oxide sand papers. Wait for at least four hours for hydration of the surfaces so that the oxide layer is formed back on the surface. Ensure the same surface roughness of all the samples for consistent results of the lap shear test.
3. Silane the surfaces using B2408 silane. Let the surfaces cure for 24 hours at room temperature.
4. Make mold on the bonding face of the strip using 3/32" thick rubber strips. The mold should be able to form 1" x 0.5" x 3/32" bracket to hold the poured 0.5 % GR/PU composite.
5. Make 0.5% GR/PU composite and pour it into the mold

6. Place the other plate onto the mold and let it cure for 36 hours.

3.2.3 Test Procedure

The tests were conducted on an Instron 8800 Servo hydraulic testing system as shown in figure 3.8. Before loading the sample on the machine, the length and width of the lap joint of every sample was measured by using vernier caliper. Gripping length of each sample in the grips was kept constant to be 1” for all samples. Figure 3.8 shows the specimen held firmly in the grips of the Instron testing machine. For all the samples, the crosshead was set to move downwards at 0.05 mm/min. The data was gathered using the software, and transferred into a spreadsheet. The test continued until fracture of the lap joint, when the control software stopped the moving crosshead, and finished gathering data. The specimen was removed, and the crosshead was reset to the initial position to start another lap shear test.



Figure 3.8 : Lap shear test specimen loaded in an Instron load frame.

3.2.4 Lap Shear Test Results

3.2.4.1 Force vs. Displacement Plots

The data file obtained after the test through Instron Data Acquisition System contains the instantaneous record of force in lbs. and displacement in inches throughout the test. Figure 3.9 and Figure 3.10 shows the plots of force vs. displacement for aluminum-aluminum bonded by PU/GR composite and steel-aluminum bonded by PU/GR composite respectively.

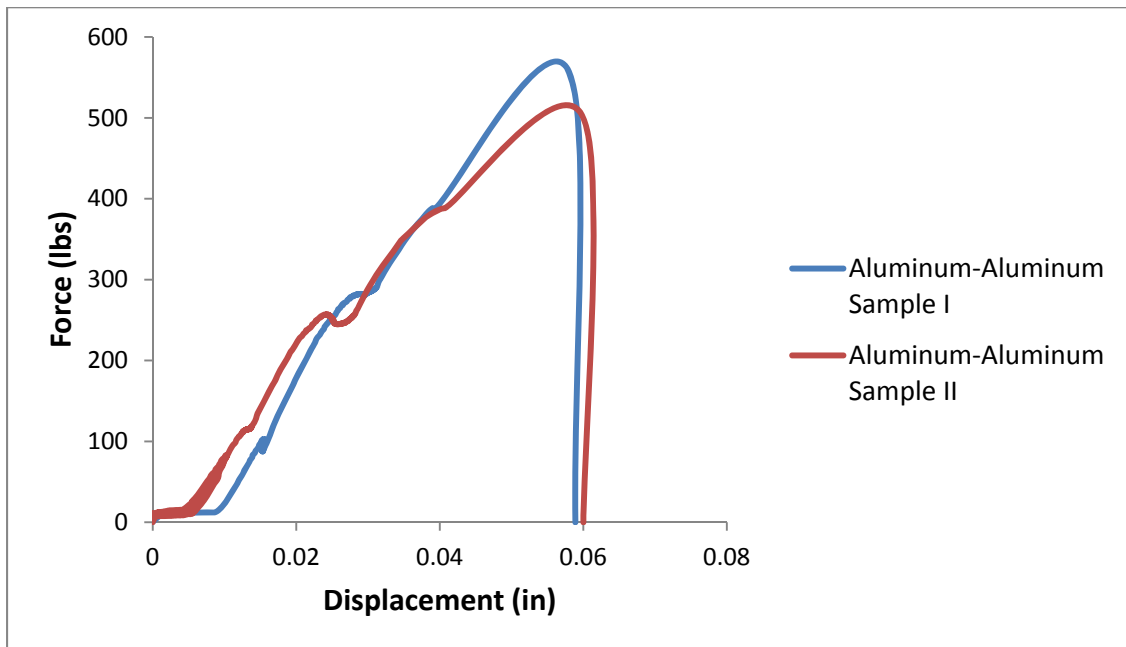


Figure 3.9 : Force vs. displacement graph for aluminum-PU/GR-aluminum samples.

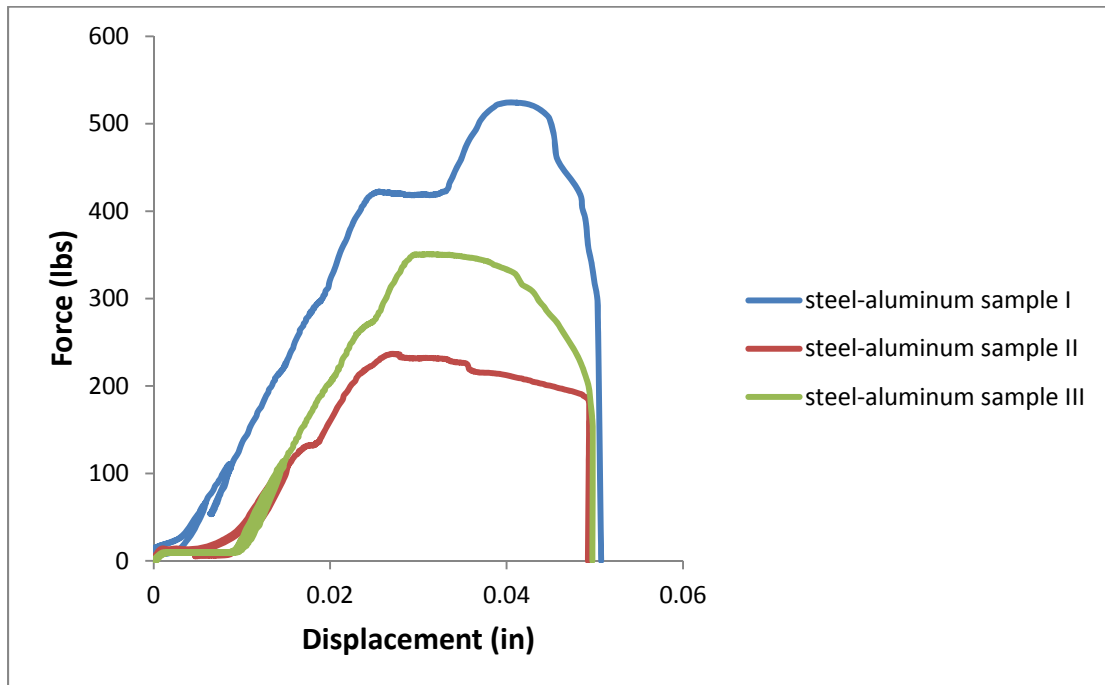


Figure 3.10 : Force vs. displacement graph for steel-PU/GR-aluminum samples.

The curves of steel-PU/GR-steel samples slightly differ from each other. Later in post analysis of samples it was found that the difference in the fracture load is due to the differences in the shear areas of the samples caused by the presence of in the adhesive metal interface. The void area was obtained by examination under an optical microscope of the sheared sample. After considering the shear area loss caused by the presence of voids, the lap shear strength of all the three test specimens was found to be consistent with each other.

3.2.4.2 Lap Shear Strength

The length and width of every sample was measured by vernier calipers before loading the sample on the machine. The shear area of every sample is calculated using equation (3.7). L

denotes the length of the overlap and w denotes the width of the overlap and A denotes the shear area.

$$A = l \times w \tag{3.7}$$

From the test data, maximum load for the fracture of the bond was determined. The lap shear strength is calculated by using the equation (3.8). σ_s denotes the lap shear strength, and F denotes fracture load.

$$\sigma_s = \frac{F}{A} \tag{3.8}$$

Table 3.2 shows the shear area and bond strength of all the lap shear test samples. It is clear from this table that the lap shear strength is fairly constant irrespective of the adherents. This proves that the lap shear strength is solely dependent on the surface treatment and surface modification processes and not on individual material combinations. The average value of lap shear strength which is 7.24 MPa has been used for the limiting shear stress value for the interaction surfaces in the ABAQUS three point bend model.

Table 3.2: Shear area and lap shear strength of all the lap shear test specimens.

| Sr. No. | Lap Shear Test Sample | Shear Area (inch²) | Failure load (lbs.) | Shear strength (psi) | Shear strength (MPa) |
|----------------|------------------------------|--------------------------------------|----------------------------|-----------------------------|-----------------------------|
| 1 | aluminum-aluminum sample-1 | 0.521 | 557.094 | 1069.687 | 7.375 |
| 2 | aluminum-aluminum sample-2 | 0.479 | 500.125 | 1043.162 | 7.192 |
| 3 | steel-aluminum sample-1 | 0.504 | 526.699 | 1045.554 | 7.209 |
| 4 | steel-aluminum sample-2 | 0.225 | 236.840 | 1050.785 | 7.245 |
| 5 | steel-aluminum sample-3 | 0.336 | 350.750 | 1042.811 | 7.190 |

3.3 THREE POINT BENDING TESTS

3.3.1 Introduction

The bend test is a simple and inexpensive qualitative test that can be used to evaluate both the ductility and stiffness of a material. It is often used as a quality control test having the advantage of simplicity of both the test piece and equipment. The bend test uses a coupon that is bent in three point bending. The three point bending test is widely used to characterize mechanical behavior of materials. The main advantage of a three point flexural test is the ease of

the specimen preparation and testing. A small beam of rectangular cross section is placed on two supports. A displacement is applied at its center and the resulting force is recorded.

In the present research work, three point bend test was carried out to learn the bending behavior of LC-1 (laminated composite-1) which is later used to validate the ABAQUS three point bending model. The test has been conducted as per standard ASME D7250/D7250M-06 [38] and was performed on the Instron 8800 servo hydraulic machine. The three point fixture with the sample is shown in Figure 3.11.



Figure 3.11 : Three point bend fixture.

3.3.2 Sample Preparation

12" x 12" LC-1 was fabricated as per the procedure given in section 2.2. The dimensions of three point bend test sample are selected as per the standard ASME D7250/D7250M-06 .Three samples of size 12" x 1.5" were cut from the 12" x 12" plate of laminated composite using water jet cutting.

3.3.3 Test apparatus and Procedure

The tests were conducted using an Instron 8800 Servo hydraulic testing system. A dial gage is used to measure the center point deflection of the specimen. The three point bend fixture attached to the load cell and the specimen placement is shown in Figure 3.12. The span length of the bending fixture on the Instron machine is set to 10 inches. The specimen was properly loaded in the frame and ensured that the load is applied at the center of the beam specimen. The tip of the dial gage was set at the center point of the sample and ensured that dial gage reads zero. The test was started, and the specimen was loaded, resulting in a measureable deflection at the center of the specimen. The data was gathered using the software, and loaded into a spreadsheet. The test continued until 0.3 inches of central deflection of the specimen, where the software stopped the moving crosshead, and finished gathering data. The specimen was removed, and the crosshead was reset to the initial position, to test another three point bending sample.



Figure 3.12 : Three point bend test set up on Instron testing machine.

3.3.4 Three Point Bend Test Results

The data file obtained from the Instron Data Acquisition System contains record of force and displacement values throughout the test. Figure 3.13 shows the plot of load vs. deflection of all the three samples. The reported average values of force for 0.3” deflection of LC-1 is 100.48 lbs.

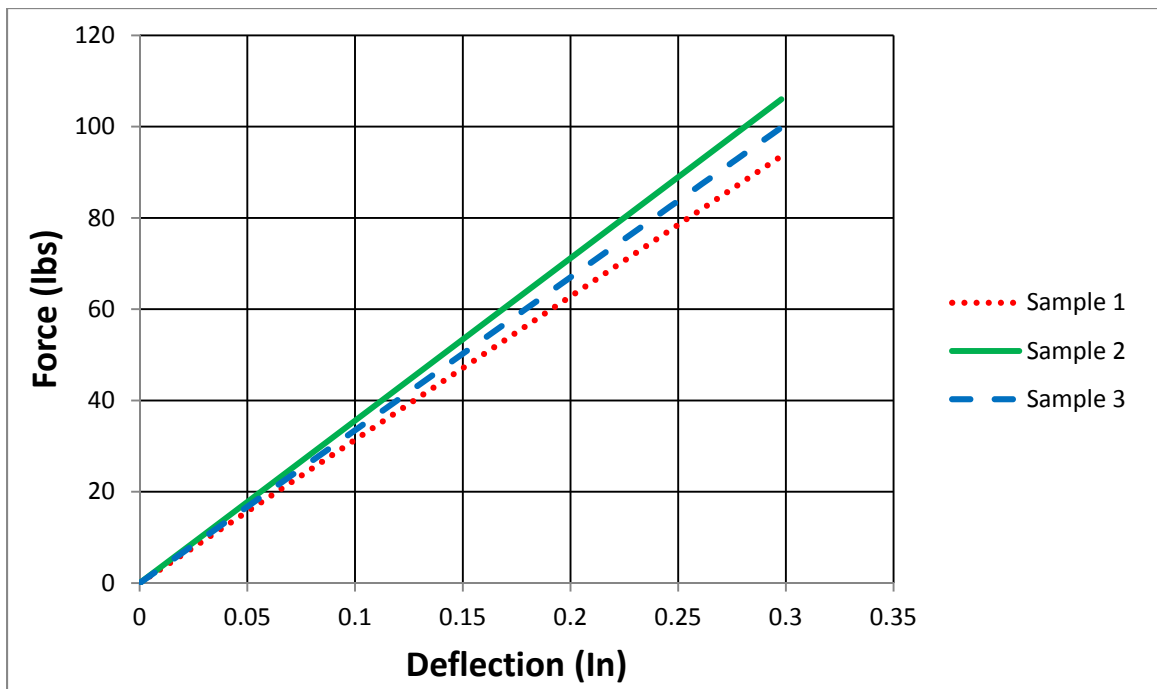


Figure 3.13 : Force vs. deflection of LC-1.

3.4 FINITE ELEMENT MODEL OF THREE POINT BEND TEST

This chapter describes the finite element simulation of three point bending using the finite element program, ABAQUS.

3.4.1 Introduction

Many researchers have used finite element software, ABAQUS, for simulation of three point bending. Steeves et al. [39] have studied the collapse mechanisms for simply supported sandwich beams with composite faces and a PVC foam core subjected to three point bending. ABAQUS is used for finite element simulation of the three point bending test. Only half of the beam is modeled due to the symmetry. The three-sided plane stress elements are used. Two reasons have been provided for using the plain stress elements. A) The foam core as it is constrained by the face sheets and behaves in plain stress manner. B) The faces are much wider than their thickness, and anti-clastic curvature is constrained by the cylindrical rollers. A good agreement was found between the experimental results and FEA simulation results. Xianyu et al. [40] used ABAQUS to simulate the fractural behavior of grade C30 concrete beams under a three-point loading configuration. ABAQUS elements CPS4R (plane stress 4—node simplified integral element) are used in this simulation. The cylindrical rollers were simulated by analytical rigid bodies. The numerical results matched well with the experimental values. Zhao et al. [41] used ABAQUS for simulation of cyclic three point bending tests on mild steel and high strength steel. Zhao et al simulated the three point bending problem by using contact simulation. The support and loading rollers were modeled by rigid analytical bodies and displacement boundary conditions are applied on the loading roller to simulate the motion of the roller. The simulation results were reported to be consistent with the experimental results.

3.4.2 Material Properties

All the materials were modeled by ABAQUS standard elastic and plastic materials. Properties of the boron steel and aluminum alloys were obtained from the supplier. Table 3.3 shows the properties of materials used for ABAQUS modeling. Figure 3.14 to 3.17 show the engineering

stress-engineering strain curves of the boron steel, Al 7075 T-6, Al 2024 T-3 and Al 5052 H-32 respectively.

Table 3.3 : Material properties used for ABAQUS modeling.

| Material | Modulus of Elasticity in MPa | Yield Strength in MPa | Poisson's Ratio |
|-------------------|-------------------------------------|------------------------------|------------------------|
| Boron steel | 247634.00 | 1100.00 | 0.3 |
| Martensitic steel | 204968.00 | 1400.00 | 0.3 |
| 0.5% PU/GR | 42.91 | 3.20 | 0.42 |
| Al 7075 T-6 | 74000.00 | 515.00 | 0.33 |
| Al 2024 T-3 | 73400.00 | 337.00 | 0.33 |
| Al 5052 H-32 | 69500.00 | 160.00 | 0.33 |

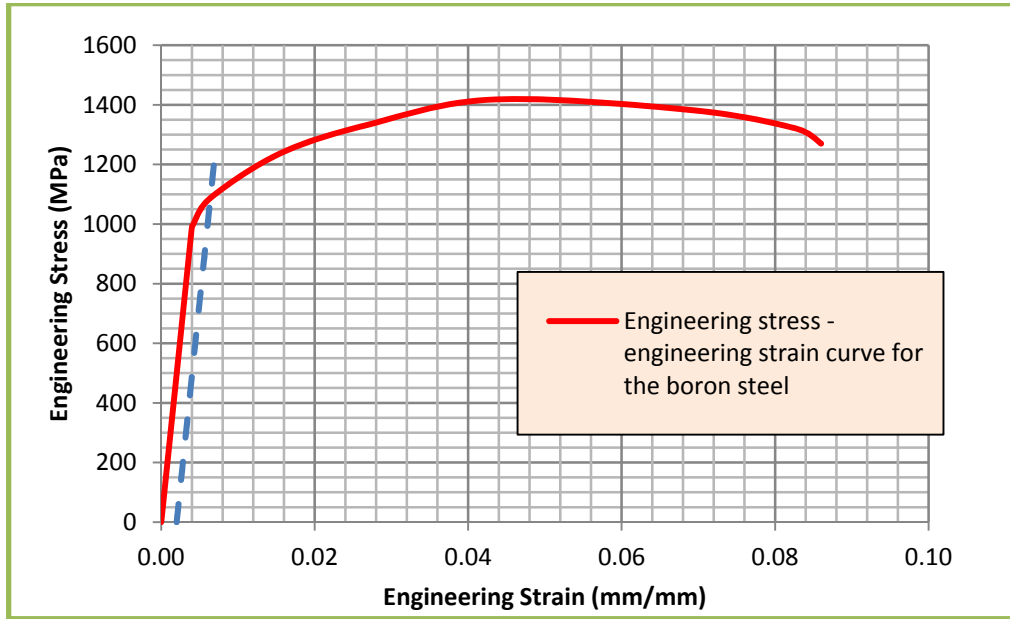


Figure 3.14 : Engineering stress - strain curve for the boron steel.

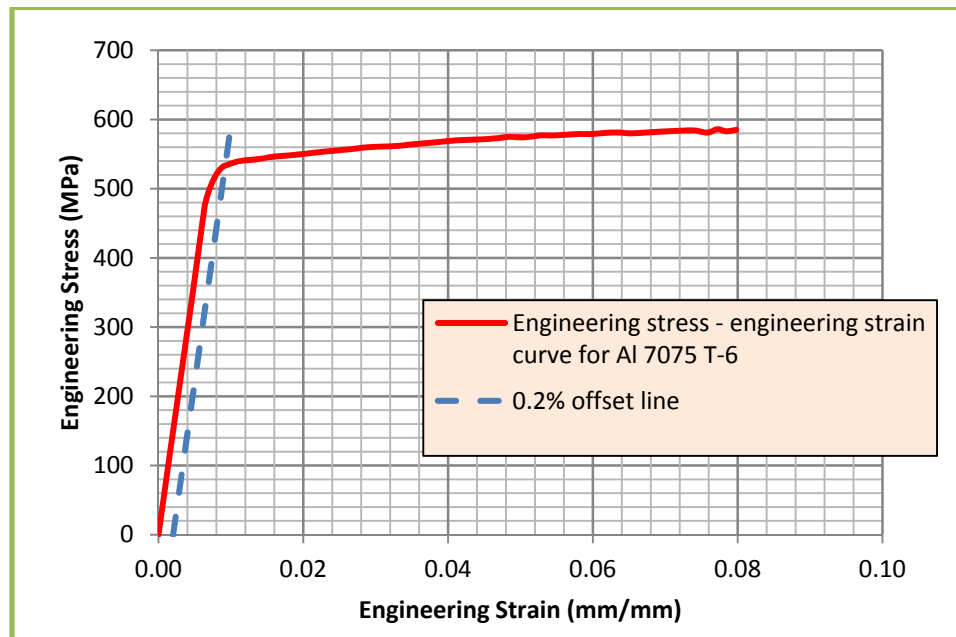


Figure 3.15 : Engineering stress - strain curve for Al 7075 T-6.

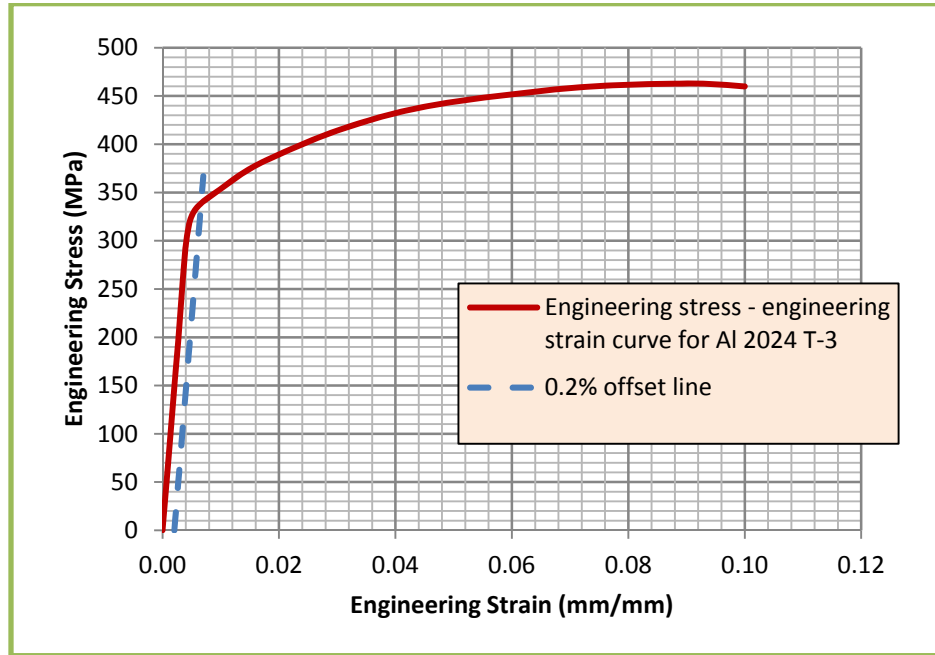


Figure 3.16 : Engineering stress - strain curve for Al 2024 T-3.

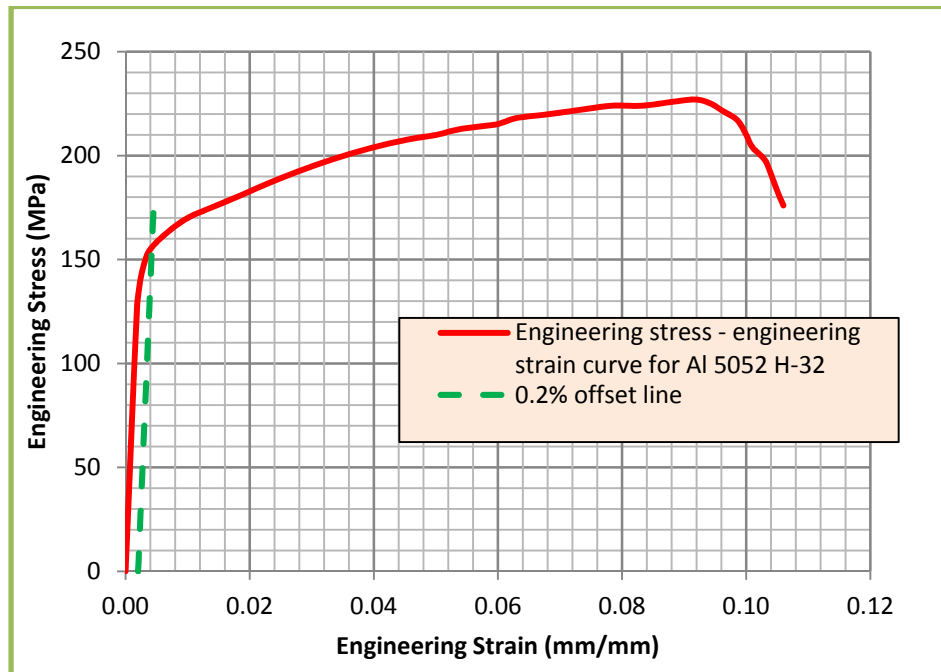


Figure 3.17 : Engineering stress - strain curve for Al 5052 H-32.

ABAQUS requires the material data in the form of true stress and true plastic strain. True stress and true plastic strain was calculated using the equation (3.4), (3.5) and (3.6) in the section 3.1.4.3. Figure 3.18 to 3.21 show the trues stress-true plastic strain curves of the boron steel, Al 7075 T-6, Al 2024 T-3 and Al 5052 H-32 respectively. The trues stress-true plastic strain curves of the martensitic steel and 0.5% PU/GR composite are shown in the previous section.

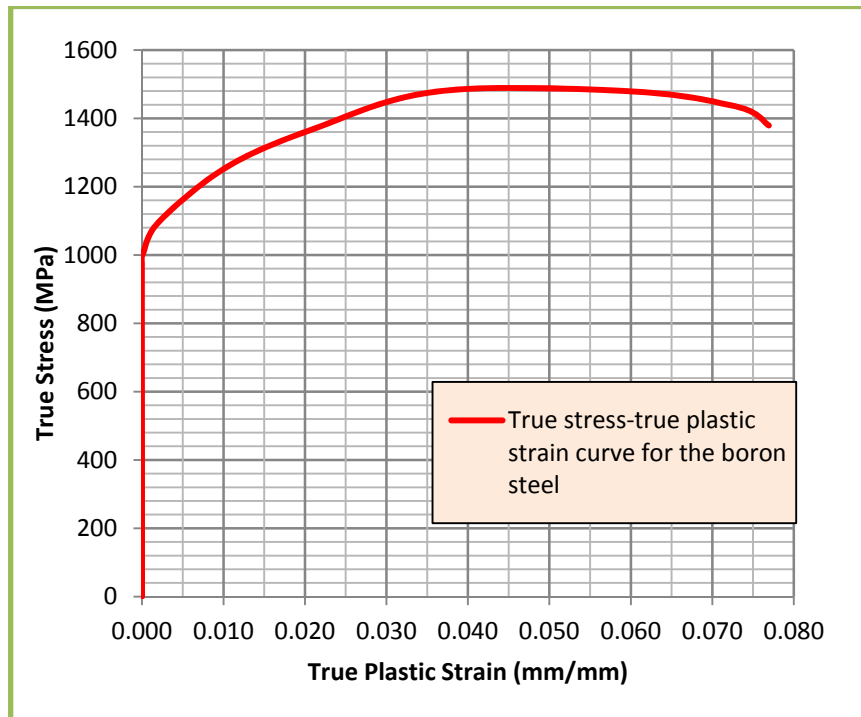


Figure 3.18 : True stress-true plastic strain curve for the boron steel.

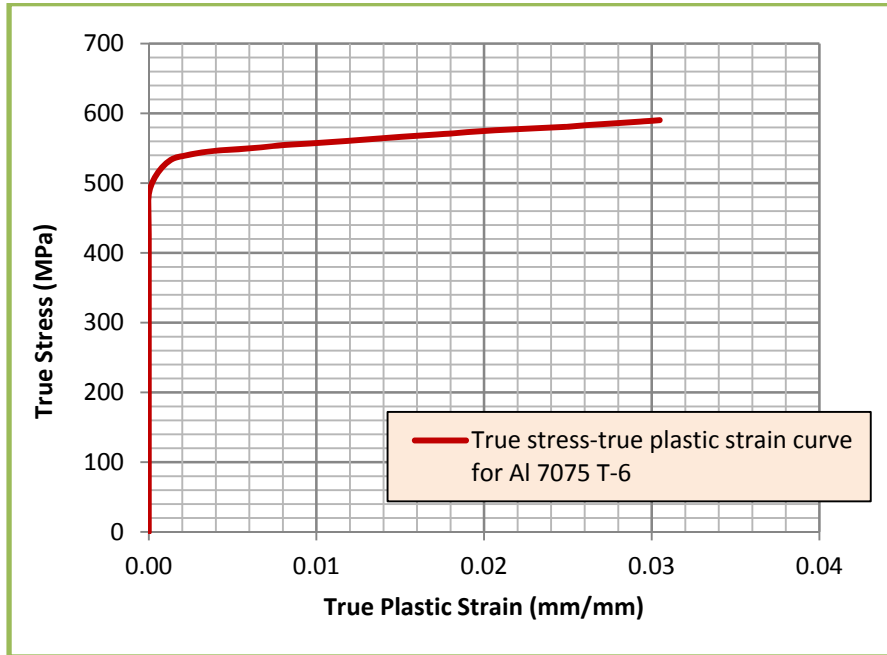


Figure 3.19 : True stress-true plastic strain curve for Al 7075 T-6.

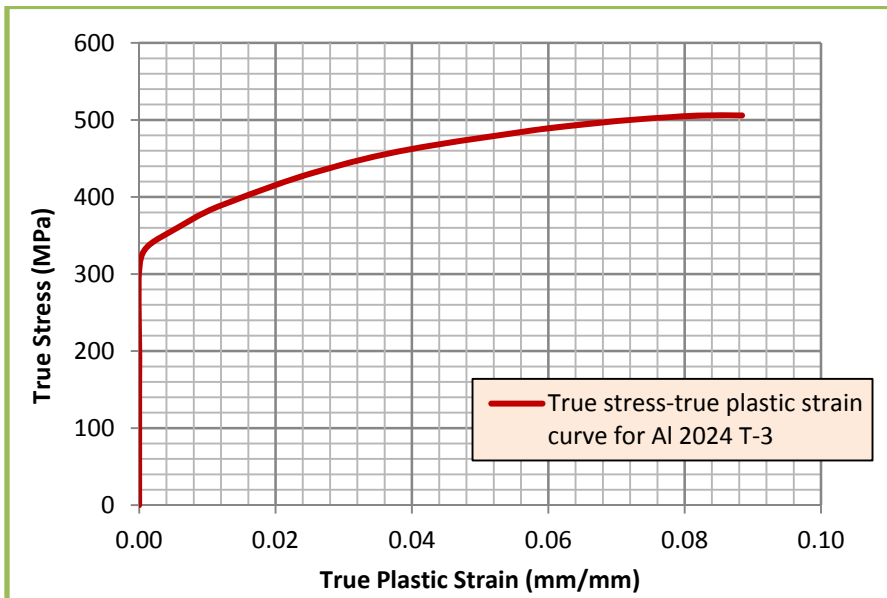


Figure 3.20 : True stress-true plastic strain curve for Al 2024 T-3.

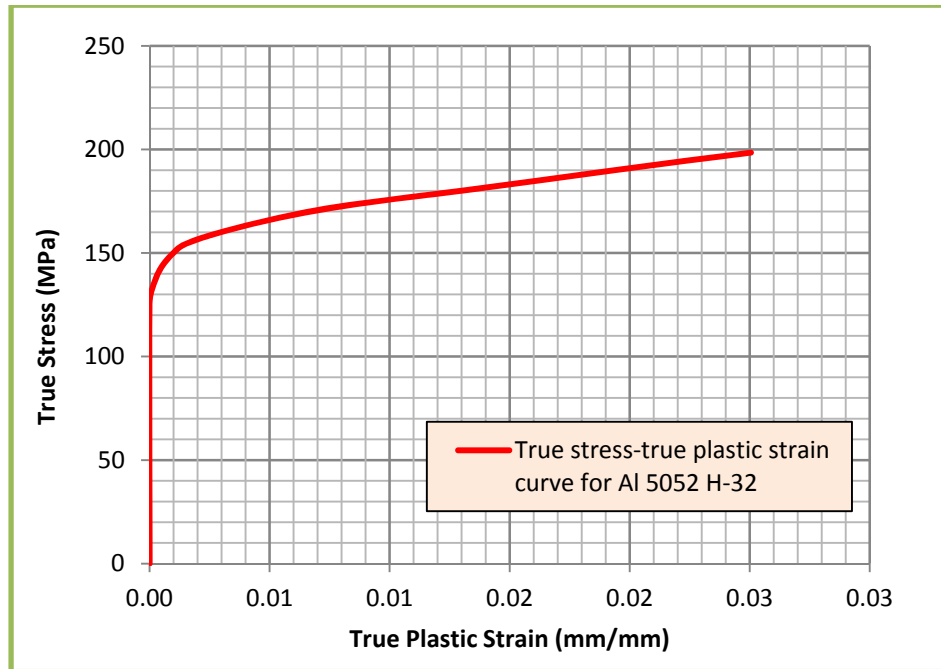


Figure 3.21 : True stress-true plastic strain curve for Al 5052 H-32.

3.4.3 Three Point Bend Test Modeling Approach

Each layer was modeled separately by ABAQUS 2D planner shell geometry. The problem was approximated to be a plane stress problem as the anti-clastic bending of the beam is constrained by the cylindrical rollers. The supporting roller and loading roller were modeled by analytical rigid bodies. Only half portion of the beam was modeled considering the symmetry. Figure 3.22 shows the assembled model geometry in ABAQUS.

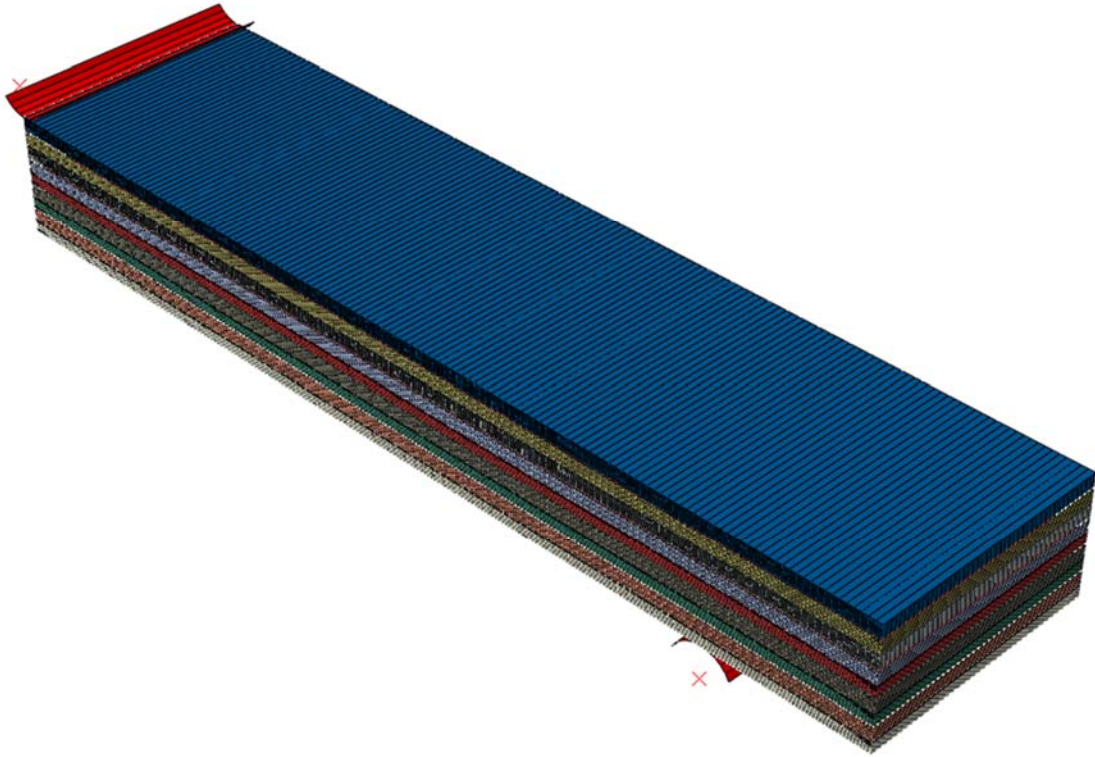


Figure 3.22 : ABAQUS model assembly.

All the degrees of freedom of the supporting roller were constrained by setting all displacement and rotational degrees of freedom to zero through boundary conditions. All the degrees of freedom except the displacement in Y direction, which is the vertical direction, of loading roller were constrained. Loading roller was set to move downwards by 0.3 inch distance by setting the boundary condition U2 (displacement in Y direction) as negative 0.3 inch. ABAQUS standard surface-surface contacts were used to define the interaction between all the mating surfaces. The contact between the beam and the rollers was set to be frictionless. Trial and error method has

been used for estimating the coefficient of friction between PU/GR and metal surfaces. It was found that at the value 4.5 of coefficient of friction, the results from FEM simulation matched closely with the experimental results. The limiting shear strength was set to be equal to the lap shear strength (7.24 MPa) obtained from lap shear testing. No slip will occur between the surfaces below the lap shear strength 7.24 MPa. The model was Meshed by using CPS4I (a 4-node bilinear plane stress quadrilateral, incompatible modes) elements with 10 elements in the thickness direction, 150 elements in the lateral direction in case of metals and 300 elements in the lateral direction for PU/GR composite layer. Finer mesh density for the PU/GR composite was selected as it was chosen to be the slave surface while defining the contact interaction and the slave surface has to be meshed finer than the master surfaces which were metal plates in this case. Figure 3.23 shows the zoomed portion meshed model.

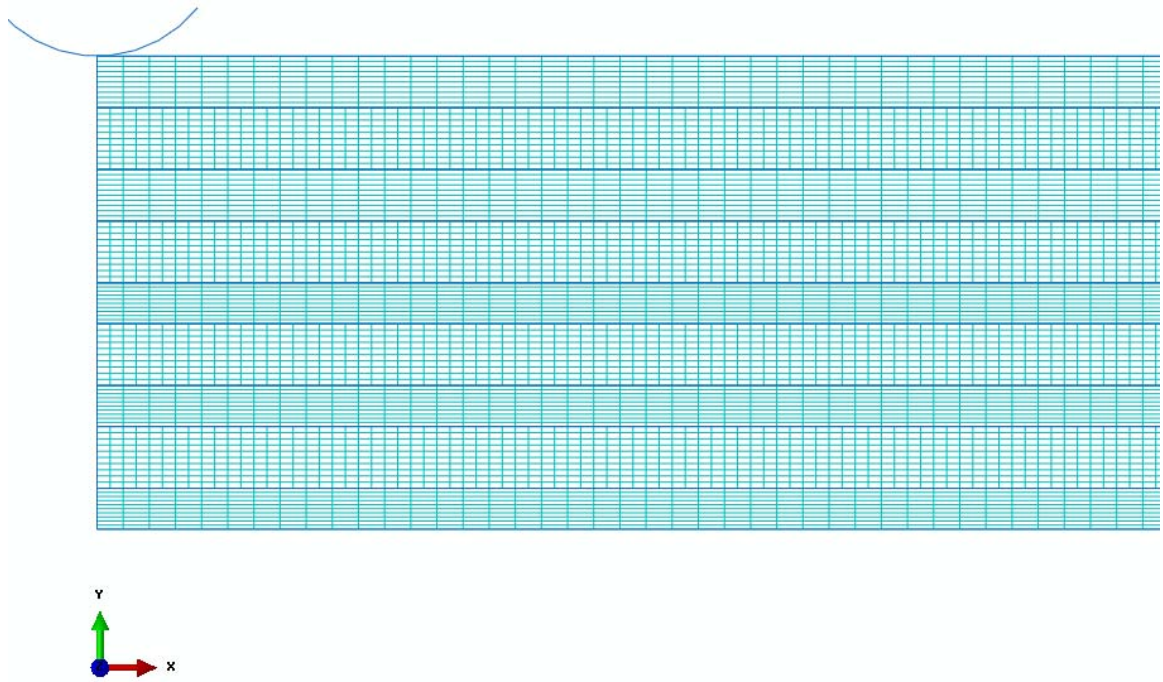


Figure 3.23 : Meshed ABAQUS model (zoomed for better view).

3.4.4 Three Point Bend Test Modeling Results

First of all, the material model developed in ABAQUS was validated by comparing the force vs. deflection plots with those obtained experimentally and then the bending behavior of all LC's is studied in ABAQUS.

3.4.4.1 Validating material model

For validating the FEM model developed in ABAQUS, the results were compared with the experimental results of three point bending test conducted on LC-1.

As explained in the three point bending testing section, three samples of LC-1, which is the martensitic steel/Al 7075 T-6/Al 2024 T-3/ Al 5052 H-32 bonded by PU/GR composite, were tested for three point bending and results were plotted as force vs. deflection. Figure 3.24 shows the force vs. deflection results from ABAQUS and those from experiments. It is clear from the figure that ABAQUS results are in good agreement with the experimental results. The percentage error in the results from ABAQUS model compared to experimental results was found to be 2.89% which is well within the acceptable limits. The good agreement between FEM results and the experimental results validates the material model developed in ABAQUS for FEM simulation of three point bending.

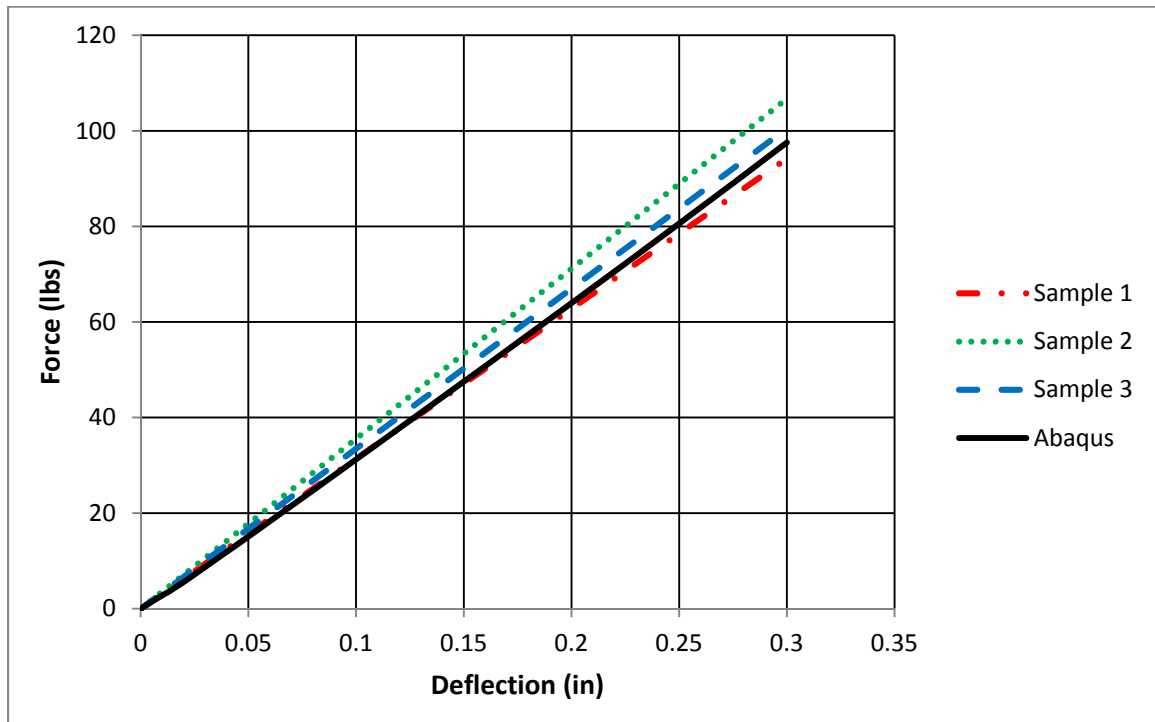


Figure 3.24 : Comparing the ABAQUS results with the experimental results for LC-1.

3.4.4.2 Bending behavior of four different configurations of laminated composites

After validating the selected material model, the remaining three LC's were modeled in ABAQUS. Figure 3.25 shows the bending behavior of all the four types of laminated composites.

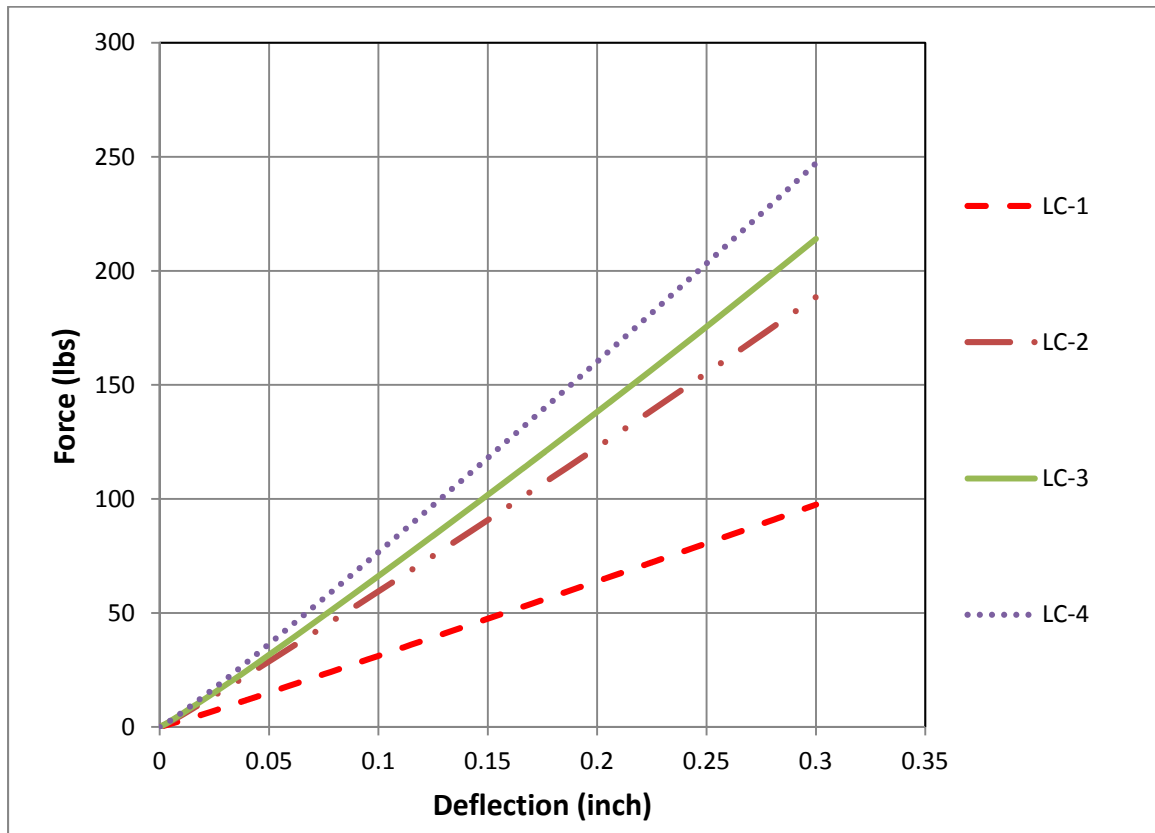


Figure 3.25 : Force vs. deflection plot obtained from ABAQUS FEM simulation.

The bending stiffness of the beams of LC-1, LC-2, LC-3 and LC-4 was calculated by using Equation (3.9) where P denotes the force and L denotes the span length.

$$\text{Bending stiffness} = \frac{P \times L^3}{48 \times \text{center point deflection}} \quad 3.9$$

Table 3.4 shows the bending stiffness of the composite beams.

Table 3.4 : Bending stiffness of composite beams.

| Material | Force (lbs) | Span length (in) | Center point Deflection (in) | Bending Stiffness of Beam (lbs x in²) |
|-----------------|--------------------|-------------------------|-------------------------------------|---|
| LC-1 | 97.56 | 10 | 0.3 | 6774.77 |
| LC-2 | 188.59 | 10 | 0.3 | 13096.18 |
| LC-3 | 213.99 | 10 | 0.3 | 14860.34 |
| LC-4 | 247.27 | 10 | 0.3 | 17171.59 |

As predicted by the ABAQUS simulation, it is seen that the LC-4 which has boron steel/boron steel as first two metal layers has the highest stiffness. The maximum stiffness of this composite is due to the boron steel which is harder than the martensitic steel. The lowest stiffness is shown by the LC-1 which was obvious as it is a 7-layer composite while all others are of 9-layers. Among the LC-3 and LC-2, which have boron steel/martensitic steel and martensitic steel/martensitic steel as the first two metal layers respectively, LC-3 is found to be stiffer as it has the boron steel frontal face which is stronger than the martensitic steel.

3.5 BALLISTIC TESTING

3.5.1 Introduction

Laminated composites structures are being widely used in military and aerospace industries due to their high ballistic resistance and light weight compared to monolithic armors. Generally when a laminated composite structure is subjected to ballistic impact, part of the energy associated with the impact is used for the elastic deformation of the material. The remaining energy in excess is

dissipated through several mechanisms like plastic deformation and delamination in the face sheets [42]. The main purpose of this work is to develop a light weight laminated composite having high ballistic resistance. This section explains the ballistic testing carried out on the laminated composite.

3.5.2 Test configuration

Two different configurations of laminated composites (LC-4 and LC-3) as shown in figure 1.4 and figure 1.3 were fabricated. Ballistic test was carried out on these laminated composites as per the ballistic test standard BTS-005. As per the ballistic testing standard BTS-005, the laminated composites were tested with 0.30 inch M80 bullets with a specified mass of 148.37 grains (9.62 grams) and a velocity of 2847 feet/s.

3.5.3 Test Results

Figure 3.26, 3.27, 3.28 and 3.29 shows pictures of the laminated composite plates after the ballistic testing. Figures 3.28 and 3.29 show the strike face and the back face of LC-4 respectively. Figures 3.30 and 3.31 show the strike face and the back face of LC-3 respectively. The bullets penetrated completely through both the composite plates and no noticeable difference between the failure patterns of the two different composite plates was found. The ballistic tests suggest that some measures need to be taken to improve the ballistic resistance of these laminated composites. The recommendation to improve the ballistic resistance are discussed in the next chapter.

Bullet Impact

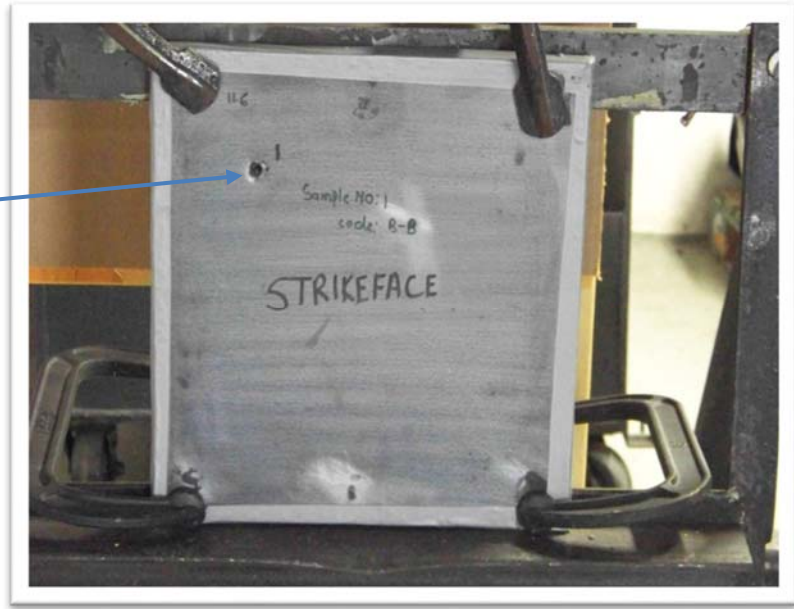


Figure 3.26 : Picture showing entering projectile damage of strike face of LC-4.



Figure 3.27 : Picture showing projectile impact damage of rear face of LC-4.

Bullet Impact

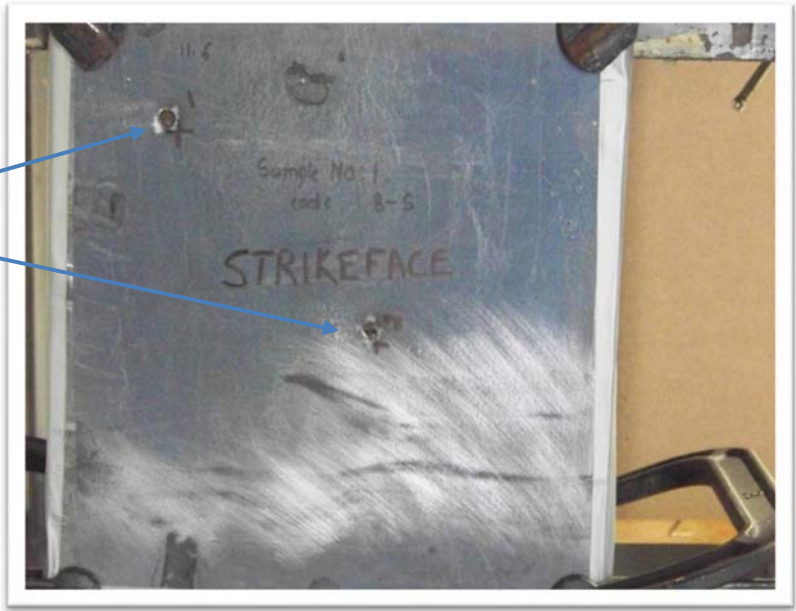


Figure 3.28 : Picture showing entering projectile damage of strike face of LC-3.



Figure 3.29 : Picture showing projectile impact damage of rear face of LC-3.

4 COLCLUSIONS AND FUTURE WORK

The primary objective of this research work was to achieve resistance against armor piercing bullet impact while keeping the weight of the composite panel at or below 10 lb/ft². To achieve this weight requirement, the cost effective standard materials such as martensitic steel, boron steel and aluminum plates were used. Other potential options are the use of ceramics such as spinel and silicon nitride, however these are order of magnitude more expensive than the other metals used in this study. The expected application of these panels is in the hard armors. Changing the face plates, four different configurations of laminated composite (LC) panels sized 12" x 12"x 0.55" for 7-layer LC and 12" x 12"x 0.75" for 9-layer LC were fabricated in this work. The metal plates were bonded to each other by 2.4 mm layer of 0.5% GR/PU composite. The average weight of the 7-layer laminated composite was found to be 7 lb. and that of 9-layer laminated composites was found to be 10 lb. for 1 ft² of the laminate.

Different tests have been conducted on the fabricated panels to determine their mechanical properties and impact behavior. Tensile testing was carried out on the martensitic steel and 0.5% PU/GR composite materials to determine the tensile properties of these materials. Lap shear tests were done on aluminum/PU-GR/aluminum and aluminum/PU-GR/steel to find out the lap shear strength of the panels. Three point bend tests were done to determine the behavior of the panel under bending loads. The finite element program, ABAQUS was used to simulate the three point bending behavior of the laminated composites. Ballistic impact tests were conducted on the panels to qualitatively measure their resistance to failure under ballistic loading.

It was observed from the three point bend test results that the laminated composite LC-4 is the stiffest of all tested LCs as first two plates, which are of the boron steel, are having high elastic modulus than those of the other three configurations of the laminated composites. LC-1 was found to be the least stiff of all testes LCs because it is 7-layer LC whereas all others are of 9-layers. Between LC-3 and LC-2, LC-3 is the stiffer one because of stiffer front face. The lap shear strength of the lap joint using PU/GR composite as adhesive layer in case of aluminum/PU-GR/aluminum and aluminum/PU-GR/steel was found to be 7.2 MPa. The same lap shear strength for both types of samples can be justified as the lap shear strength is solely dependent on the surface texture and surface modification of the bonding materials which was kept same for both the bonding materials in this research.

The ballistic test was conducted on LC-4 and LC-3 as per the ballistic testing standard BTS-005. 0.30 inch M80 bullets with a specified mass of 148.37 grains (9.62 grams) and a velocity of 2847 feet/s were shot at the specimens. The bullets penetrated both LC-4 and LC-3 completely. The failure of the plates is speculated to be due to the lower perforation resistance of the panels than required. Some measures for improving the ballistic resistance are given below.

In this work new light weight laminated composite panels have been developed. There is a lot of room for further research and analysis of these panels to improve their ballistic performance. Some of the areas that we intend to work on in the near future are:

- 1) Change the configuration of the laminated composite utilizing a harder ceramic material, as compared to the boron steel, as the frontal layer. Many laminated composites with ceramic material as a frontal layer are being developed. Ceramic, being very hard, can blunt the projectiles and reduce the velocity of projectile which can help improving the penetration resistance of the panels. An example of a ceramic layer could be silicon nitride.

2) Perform finite element analysis for analyzing the ballistic performance of the laminated composite panels using ABAQUS. This would help us further analyze the behavior of the panels under ballistic impact and also predict the damage characteristics. This would also help to figure out the optimum configuration of the laminated composites having the highest ballistic resistance and lowest weight.

3) Perform ballistic tests on all the laminated composite plates with ballistic gel blocks placed behind the rear face of the plates. This will help us assessing the effectiveness of the plates qualitatively in providing ballistic protection by measuring the penetration of the disintegrated bullet debris into the ballistic gel block.

5 REFERENCES

1. Madhu, V. and T.B. Bhat, *Armour Protection and Affordable Protection for Futuristic Combat Vehicles*. 2011. Vol. 61. 2011.
2. Ramadhan, A., et al., *High velocity impact response of Kevlar-29/epoxy and 6061-T6 aluminum laminated panels*. *Materials & Design*, 2012.
3. Hazell, P.J.A.-T., G J; Kister, G, *Impact, penetration, and perforation of a bonded carbon-fibre-reinforced plastic composite panel by a high-velocity steel sphere: an experimental study*. *The Journal of Strain Analysis for Engineering Design*, 2010. 45: p. 439-450.
4. Guoqi, Z., W. Goldsmith, and C.K.H. Dharan, *Penetration of laminated Kevlar by projectiles—I. Experimental investigation*. *International Journal of Solids and Structures*, 1992. 29(4): p. 399-420.
5. Cheng, W.L., S. Langlie, and S. Itoh, *High velocity impact of thick composites*. *International Journal of Impact Engineering*, 2003. 29(1-10): p. 167-184.
6. Guiping, Z., et al., *Experimental Study on Impact Resistance Properties of T300/Epoxy Composite Laminates*. *Journal of Composite Materials*, 2009. 44(7): p. 857-870.
7. Kumar, S., et al., *Behavior of Kevlar/Epoxy Composite Plates Under Ballistic Impact*. *Journal of Reinforced Plastics and Composites*, 2009. 29(13): p. 2048-2064.
8. Ravid, M. and S.R. Bodner, *Dynamic perforation of viscoplastic plates by rigid projectiles*. *International Journal of Engineering Science*, 1983. 21(6): p. 577-591.
9. Tan, V.B.C. and K.J.L. Khoo, *Perforation of flexible laminates by projectiles of different geometry*. *International Journal of Impact Engineering*, 2005. 31(7): p. 793-810.
10. Wang, L. and X. Zhang, *Collision Ansysis of Sandwiched Polyurethane Composite Steel Tube*. *Advanced Materials Research*, 2012. 535-537: p. 194-200.
11. Wentworth, S.E., et al., *Synthesis and Ballistic Evaluation of Selected Transparent Polyurethane Block Copolymers*. 1973, ARMY MATERIALS AND MECHANICS RESEARCH CENTER WATERTOWN MASS.
12. Fountzoulas, C., et al., *A computational study of laminate transparent armor impacted by FSP*. 2009, DTIC Document.

13. Hepburn, C., *Trends in polyurethane elastomer technology*. Iranian Journal of Polymer Science and Technology, 1992. 1(2).
14. Alpay Yilnaz, A., Turkey, *Development of an armor steel for ballistic protection*. Materials Testing, 2010. 52(11): p. 811-818.
15. Crouch, I.G., *Metallic armour - from cast aluminium alloys to high-strength steels*. Materials Forum. 12: p. 1988.
16. Übeyli, M., et al., *Ballistic impact performance of an armor material consisting of alumina and dual phase steel layers*. Materials & Design, 2011. 32(3): p. 1565-1570.
17. Ade, F., *Ballistic qualification of armor steel weldments*. 1991, GENERAL DYNAMICS CORP STERLING HEIGHTS MI LAND SYSTEMS DIV.
18. Sangoy, L., Y. Meunier, and G. Pont, *Steels for ballistic protection*. Israel journal of technology, 1988. 24(1-2): p. 319-326.
19. Gooch, W., M. Burkins, and R. Squillacioti. *Ballistic Testing of Commercial Aluminum Alloys and Alternate Processing Techniques to Increase the Availability of Aluminum Armor*. in *23rd International Symposium on Ballistics, Tarragona, Spain*. 2007.
20. Phan, H.T., *High strain rate behavior of graphene reinforced polyurethane composites*. 2012, University of Missouri.
21. Khan, U., F.M. Blighe, and J.N. Coleman, *Selective mechanical reinforcement of thermoplastic polyurethane by targeted insertion of functionalized SWCNTs*. Journal of Physical Chemistry C, 2010. 114(26): p. 11401-11408.
22. Kim, H., Y. Miura, and C.W. MacOsco, *Graphene/polyurethane nanocomposites for improved gas barrier and electrical conductivity*. Chemistry of Materials, 2010. 22(11): p. 3441-3450.
23. Wong, H.-S.P. and D. Akinwande, *Carbon nanotube and graphene device physics*. 2011, Cambridge ; New York: Cambridge University Press. x, 251 p.
24. Geim, A.K. and K.S. Novoselov, *The rise of graphene*. Nature materials, 2007. 6(3): p. 183-191.
25. Kuilla, T., et al., *Recent advances in graphene based polymer composites*. Progress in Polymer Science, 2010. 35(11): p. 1350-1375.
26. Zhao, X., et al., *Enhanced mechanical properties of graphene-based polyvinyl alcohol composites*. Macromolecules, 2010. 43(5): p. 2357-2363.
27. Lee, H.-i. and H.M. Jeong, *Functionalized Graphene Sheet/Polyurethane Nanocomposites*. Polym Polym Compos, 2010. 18: p. 351-358.

28. Wang, X., et al., *In situ polymerization of graphene nanosheets and polyurethane with enhanced mechanical and thermal properties*. J. Mater. Chem., 2011. 21(12): p. 4222-4227.
29. Nguyen, D.A., et al., *Morphological and physical properties of a thermoplastic polyurethane reinforced with functionalized graphene sheet*. Polymer International, 2009. 58(4): p. 412-417.
30. Arenas, J.M., et al., *Considerations for the industrial application of structural adhesive joints in the aluminium-composite material bonding*. Composites Part B: Engineering, 2013. 44(1): p. 417-423.
31. ASM International. Handbook Committee. and Knovel (Firm), *ASM handbook. Volume 2, Properties and selection: nonferrous alloys and special-purpose materials*. 1990, ASM International,: Materials Park, OH. p. 1 online resource (xv, 1328 p.).
32. MIL-DTL-46063H, M.S., *Armor Plate, Aluminum Alloy, 7039*. AMSRL-WM-MA, US Army Research Laboratory, (14 September 1998).
33. MANGENELLO, S. and K. Abbott, *Metallurgical factors affecting the ballistic behavior of steel targets*. J MATER, 1972. 7(2): p. 231-239.
34. Handbook, A., *Properties and selection: irons, steels, and high performance alloys*. ASM International, 1990. 1: p. 140-194.
35. Standard, A., *E8," Standard Test Methods for Tension Testing of Metallic Materials*. Annual book of ASTM standards, 2001. 3: p. 57-72.
36. Standard, A., *D638: Standard Test Method for Tensile Properties of Plastics*. ASTM International, West Conchohocken, 2008.
37. Astm, D. *1002-10 Standard Test Method for Apparent Shear Strength of Single-Lap-Joint Adhesively Bonded Metal Specimens by Tension Loading (Metal-to-Metal)-ASTM*. 2010. International.
38. Testing, A.S.f. and M. Philadelphia, *Standard practice for determining sandwich beam flexural and shear stiffness*. 2006.
39. Steeves, C.A. and N.A. Fleck, *Collapse mechanisms of sandwich beams with composite faces and a foam core, loaded in three-point bending. Part II: experimental investigation and numerical modelling*. International Journal of Mechanical Sciences, 2004. 46(4): p. 585-608.
40. Jin, X., N. Jin, and Y. Zheng, *FRACTURAL MODELLING OF EARLY-AGE CONCRETE BEAMS UNDER THREE-POIN LOADING*.
41. Zhao, K. and J. Lee, *Finite element analysis of the three-point bending of sheet metals*. Journal of materials processing technology, 2002. 122(1): p. 6-11.

42. **Johnson, A. and M. Holzapfel, *Influence of delamination on impact damage in composite structures*. Composites science and technology, 2006. 66(6): p. 807-815.**